Laser and Particle Beams (2016), *34*, 576–600.

doi:10.1017/S0263034616000495

Vlasov–Maxwell simulations of backward Raman amplification of seed pulses in plasmas

MAGDI SHOUCRI[1] AND BEDROS AFEYAN[2]

[1]Institut de recherche d'Hydro-Québec (IREQ), Varennes, Québec J3X1S1, Canada
[2]Polymath Research Inc., Pleasanton, CA 94566, USA

(Received 11 April 2016; Accepted 2 August 2016)

Abstract

We study the problem of the amplification of an ultra-short seed pulse via stimulated Raman backscattering (SRB) from a long pump pulse (assumed to have an envelope with a constant amplitude), in an underdense plasma. The SRB interaction couples the pump light wave to a daughter light seed wave propagating in the opposite direction, scattered off an electron plasma wave. In recent numerical simulations, it has been observed that besides stimulated Raman backward scattering (SRBS) and stimulated Raman forward scattering, other high-frequency kinetic instabilities can occur when modified distribution functions exist during the evolution of the system. In particular, we showed the prominent role played by kinetic electrostatic electron nonlinear (KEEN) waves (Afeyan *et al.*, 2004). We continue this work by applying a relativistic Vlasov–Maxwell code to study stimulated KEEN wave scattering (SKEENS) and its role in the SRBS short pulse amplification processes. An analysis of the full spectrum of waves participating in the amplification processes is presented. The absence of spurious noise in grid-based Vlasov codes allows us to follow the evolution of the system with a kinetic (collisionless) description. This affords us a glimpse at the intricate phase-space structures such as trapped particle orbits, which coexist and interact nonlinearly in the electron distribution function.

Keywords: Laser–plasma instabilities; Raman backward amplification; Stimulated KEEN wave scattering; Stimulated Raman Scattering; Trapped particle distribution functions

1. INTRODUCTION

Three-wave parametric interactions in plasmas involve the coupling of two transversely polarized electromagnetic waves and a longitudinally polarized plasma wave. They have been extensively studied both theoretically and numerically using plane waves models (see, for instance, Drake *et al.*, 1974; Max *et al.*, 1974; Forslund *et al.*, 1975; Spatschek, 1976; Kruer, 1988). In stimulated Raman scattering, the plasma response is that of a high-frequency electron plasma wave (EPW), while in Brillouin scattering it is a low-frequency ion acoustic wave (IAW). These processes have also received considerable attention in the context of generating ultra-intense and ultra-short laser pulses (see, for instance, Ren *et al.*, 2007; Mourou *et al.*, 2012; Riconda *et al.*, 2013). In these new developments transient pulse, propagation effects become important, and involve the collision of an ultra-short seed pulse with a long pump pulse, in order to amplify the seed pulse intensity by several orders of magnitude. In the amplification process, the long pump pulse of high energy but moderate intensity propagating in an underdense plasma collides with a short seed pulse of either smaller or higher-intensity propagating in the opposite direction. The seed pulse convectively grows with interaction distance as does the plasma mode (EPW or IAW). But as the seed pulse grows, it eventually depletes the pump field. The use of plasma as an amplifying medium is needed so as to achieve ultra-high light intensities via plasma optics, with laser beams operating in the exawatt and zetawatt regimes (Mourou *et al.*, 2012). Promising experimental results have been reported on the way to that ultimate regime (Ren *et al.*, 2007; Mourou *et al.*, 2012; Riconda *et al.*, 2013; Lancia *et al.*, 2010; Trines *et al.*, 2011*a*, *b*). Stimulated Raman amplification has been examined in several publications (Malkin *et al.*, 1999, 2014; Fisch & Malkin, 2003; Malkin & Fisch, 2005; Benisti *et al.*, 2012), and more recently in several numerical simulations (Wang *et al.*, 2010; Trines *et al.*, 2011*a*, *b*; Lehmann *et al.*, 2012, 2013; Lehmann & Spatschek, 2013, 2014; Toroker *et al.*, 2014).

Address correspondence and reprint requests to: M. Shoucri, Institut de recherche d'Hydro-Québec (IREQ), Varennes, Québec J3X1S1, Canada. E-mail: shoucri.magdi@ireq.ca

In other recent simulations, it has been shown that besides stimulated Raman backward scattering (SRBS) and stimulated Raman forward scattering (SRFS), other high-frequency kinetic instabilities can occur when modified distribution functions exist during the evolution of the system. In the family of such structures a particularly prominent role is played by kinetic electrostatic electron nonlinear (KEEN) waves (Afeyan *et al.*, 2004, 2014; Mehrenberger *et al.*, 2013) whose role in dictating the dynamics of SRS was examined in (Shoucri & Afeyan, 2014). These stimulated processes are called SKEENS. There have also been associations made between beam acoustic modes BAM (Yin *et al.*, 2006; Strozzi *et al.*, 2007, 2010) and SRBS' nonlinear evolution. A different perspective has also been promulgated under the heading of transient enhanced instability levels attributed to rapidly changing distribution functions which diminish damping rates and thus allow larger levels of SRS than would be expected in models ignoring transient tracking of distribution functions. That trend began with the work of Afeyan *et al.* (1998) invoking nonlocal heat transport and filamentation as root causes of distribution function changes and continued under the heading of inflationary models (Vu *et al.*, 2007). Of these KEEN waves have the interesting features that they do not require a pre-flattened (zero slope at the phase velocity of the wave) distribution function and are not steady state, time-independent solutions (Afeyan *et al.*, 2004, 2014; Mehrenberger *et al.*, 2013). KEEN waves are not single mode structures, but multimode, self-organized non-stationary states of Vlasov plasmas. In particular, they can be driven anywhere inside the spectral gap in plasma (linear response) theory below the EPW dispersion curve and above the IAW one. An electron acoustic waves EAW (Sircombe *et al.*, 2006; Valentini *et al.*, 2006), in contrast, is strictly and rather delicately limited to yet another linear dispersion curve at a slope (i.e. with a phase velocity) of around $1.3\times$ the thermal velocity of electrons. EAWs constitute a set of measure zero compared with KEEN waves in the drive (ω, k) plane or Brillouin diagram. EAWs require a flat distribution function of zero slope at the phase velocity of the driven wave which is very delicate to set up, is by construction single mode, and stationary unlike KEEN waves which obey none of these artificial (simplifying) restrictions.

In the work reported here, we utilize a Vlasov–Maxwell code to study the problem of the amplification of an ultrashort seed pulse via stimulated Raman backscattering (SRB) of energy from a long pump pulse at a slightly higher frequency (and assuming it has a fixed amplitude). We identify the KEEN wave contribution in the Raman scatter of energy for pulse amplification, in a way similar to what has been presented in Shoucri and Afeyan (2014). The Vlasov code we use solves the one-dimensional (1D) relativistic Vlasov–Maxwell set of equations, and has been previously successfully applied to different problems in laser–plasma interaction, such as wake field acceleration (Shoucri, 2008*a*, *b*). These codes have also been successfully applied to study stimulated Raman scattering of plane waves in an underdense plasma (Ghizzo *et al.*, 1990), and more recently to the problem of Raman seed pulse amplification in Lehmann *et al.* (2013), Lehmann and Spatschek (2014), Toroker *et al.* (2014), Shoucri *et al.* (2015), and to the problem of Brillouin seed amplification when the plasma response is provided by an IAW (Shoucri *et al.*, 2015). The absence of noise in the Vlasov code allows more accurate representation of the phase-space structures in the distribution function, and more accurate identification of the modes involved in the physics of the backscattering process. It avoids numerical problems like excessive pump scattering from numerical noise (Shoucri *et al.*, 2015).

2. THE RELEVANT EQUATIONS OF THE EULERIAN VLASOV CODE AND THE NUMERICAL SCHEME

The relevant equations for the Eulerian Vlasov code are those previously presented in references (Ghizzo *et al.*, 1990; Shoucri, 2008*a*, *b*; Shoucri *et al.*, 2015) for instance. We present these equations here again just in order to fix the notation. Time t is normalized to the inverse plasma frequency ω_{pe}^{-1}, length is normalized to $l_0 = c\omega_{pe}^{-1}$, velocity and momentum are normalized respectively to the velocity of light c and to $M_e c$, where M_e is the electron mass, and c is the velocity of light. We have the following Vlasov equations for the electrons and the ions distribution functions $f_{e,i}(x, p_{xe,i}, t)$:

$$\frac{\partial f_{e,i}}{\partial t} + \frac{p_{xe,i}}{m_{e,i}\gamma_{e,i}}\frac{\partial f_{e,i}}{\partial x} + \left(\mp E_x - \frac{1}{2m_{e,i}\gamma_{e,i}}\frac{\partial a_\perp^2}{\partial x}\right)\frac{\partial f_{e,i}}{\partial p_{xe,i}} = 0, \quad (1)$$

where the relativistic factor $\gamma_{e,i} = (1 + (p_{xe,i}/m_{e,i})^2 + (a_\perp/m_{e,i})^2)^{1/2}$.

The upper sign in Eq. (1) is for the electron equation and the lower sign for the ion equation, and subscripts e or i denote electrons or ions, respectively. In our normalized units $m_e = 1$ and $m_i = M_i/M_e = 1836$ for the hydrogen ions. In the 1D model, the normalized canonical momentum $\vec{P}$ is related to the particle momentum $\vec{p}$ by the relation $\vec{P} = \vec{p} \mp \vec{a}_\perp$, where $\vec{a} = e\vec{A}/M_e c$ is the normalized vector potential. In the direction normal to x, the canonical momentum $\vec{P}_{\perp e,i}$ is conserved and it can be chosen initially to be 0, so that $\vec{p}_{\perp e,i} = \pm\vec{a}_\perp$.

The electric field in the transverse direction is calculated from the relation:

$$\vec{E}_\perp = -\frac{\partial \vec{a}_\perp}{\partial t}. \quad (2)$$

The transverse electromagnetic fields E_y, B_z for the linearly polarized wave obey Maxwell's equations. Defining $E^\pm = E_y \pm B_z$, we have:

$$\left(\frac{\partial}{\partial t} \pm \frac{\partial}{\partial x}\right)E^\pm = -J_y. \quad (3)$$

https://doi.org/10.1017/S0263034616000495 Published online by Cambridge University Press

In our normalized units, we have the following expressions for the normal current densities:

$$\vec{J}_\perp = \vec{J}_{\perp e} + \vec{J}_{\perp i}; \quad \vec{J}_{\perp e,i} = -\frac{\vec{a}_\perp}{m_{e,i}} \int_{-\infty}^{+\infty} \frac{f_{e,i}}{\gamma_{e,i}} dp_{xe,i}. \tag{4}$$

The longitudinal electric field is calculated from Ampère's equation: $\partial E_x/\partial t = -J_x$, where

$$J_x = \frac{1}{m_i} \int_{-\infty}^{+\infty} \frac{p_{xi}}{\gamma_i} f_i dp_{xi} - \frac{1}{m_e} \int_{-\infty}^{+\infty} \frac{p_{xe}}{\gamma_e} f_e dp_{xe}. \tag{5}$$

Test runs were made in which Poisson's equation was used instead of Ampère's equation to obtain the longitudinal electric field E_x, with identical results.

The numerical scheme to advance Eq. (1) from time t_n to t_{n+1} necessitates the knowledge of the electromagnetic field $E^\pm$ at time $t_{n+1/2}$. This is done using a centered scheme where we integrate Eq. (3) exactly along the vacuum characteristics with $\Delta x = \Delta t$, to calculate $E^{\pm n+1/2}$ as follows:

$$E^\pm(x \pm \Delta t, t_{n+1/2}) = E^\pm(x, t_{n-1/2}) - \Delta t J_y(x \pm \Delta t/2, t_n) \tag{6}$$

with

$$J_y\big(x \pm \Delta t/2, t_n\big) = \frac{J_y(x \pm \Delta x, t_n) + J_y(x, t_n)}{2}.$$

From Eq. (2) we also have $\vec{a}_\perp^{n+1} = \vec{a}_\perp^{n} - \Delta t \vec{E}_\perp^{n+1/2}$, from which we calculate $\vec{a}_\perp^{n+1/2} = (\vec{a}_\perp^{n+1} + \vec{a}_\perp^{n})/2$. To calculate $E_x^{n+1/2}$, we use Ampère's equation: $\partial E_x/\partial t = -J_x$, from which $E_x^{n+1/2} = E_x^{n-1/2} - \Delta t J_x^n$.

The Eulerian Vlasov code we use to solve Eqs. (1)–(5) has been presented and applied for instance in (Shoucri, 2008*a*, *b*; Shoucri *et al.*, 2015). We outline the main steps for the numerical solution of Eq. (1), using an Eulerian scheme. Given $f_{e,i}^n$ at mesh points at time $t = n\Delta t$ (we stress here that the subscript i denotes the ion distribution function), we calculate the new value $f_{e,i}^{n+1}$ at the grid points j_x, and j_p corresponding to the mesh points (x_{j_x}, p_{xe,ij_p}) by writing that the distribution function is constant along the characteristics. We assume that at the time $t_{n+1} \equiv t_n + \Delta t$, x is at the grid point j_x, and $p_{xe,i}$ is at the grid point j_p. Let $(x(t_n), p_{xe,i}(t_n))$ is the point where the characteristic is originating at t_n (not necessarily a grid point). This point is calculated from the solution of the characteristics equations between t_n and $t_{n+1} \equiv t_n + \Delta t$:

$$\begin{aligned} \frac{dx}{dt} &= m_{e,i} \frac{p_{xe,i}}{\gamma_{e,i}} = V_{xe,i}(x, p_{xe,i}), \\ \frac{dp_{xe,i}}{dt} &= \mp E_x - \frac{m_{e,i}}{2\gamma_{e,i}} \frac{\partial a_\perp^2}{\partial x} = V_{p_{xe,i}}(x, p_{xe,i}). \end{aligned} \tag{7}$$

We assume that at the time $t_{n+1} \equiv t_n + \Delta t$, x is at the grid point j_x, and $p_{xe,i}$ is at the grid point j_p. The following leap-frog scheme can be written for the solution of (6):

$$\begin{aligned} \frac{x_{j_x} - x(t_n)}{\Delta t} &= V_{xe,i}(x^{n+1/2}, p_{xe,i}^{n+1/2}) \\ &= V_{xe,i}\left(\frac{x_{j_x} + x(t_n)}{2}, \frac{p_{xe,ij_p} + p_{xe,i}(t_n)}{2}\right). \end{aligned} \tag{8}$$

$$\begin{aligned} \frac{p_{xe,ij_p} - p_{xe,i}(t_n)}{\Delta t} &= V_{p_{xe,i}}(x^{n+1/2}, p_{xe,i}^{n+1/2}) \\ &= V_{p_{xe,i}}\left(\frac{x_{j_x} + x(t_n)}{2}, \frac{p_{xe,ij_p} + p_{xe,i}(t_n)}{2}\right). \end{aligned}$$

These equations are solved by iteration for:

$$\Delta_x = \frac{x_{j_x} - x(t_n)}{2}; \quad \Delta_{p_{xe,i}} = \frac{p_{xe,ij_p} - p_{xe,i}(t_n)}{2}.$$

From which $x(t_n) = x_{j_x} - 2\Delta_x$, $p_{xe,i}(t_n) = p_{xe,i} - 2\Delta_{p_{xe,i}j_p}$. We now write that the distribution function is constant along the characteristics. Then $f_{e,i}^{n+1}(x_{j_x}, p_{xe,ij_p})$ is equal to $f_{e,i}^n(x(t_n), p_{xe,i}(t_n))$, this latter value is calculated from the values of $f_{e,i}^n$ at the grid points by a 2D interpolation using a tensor product of cubic B-splines (for details, see Shoucri *et al.*, 2003; Shoucri, 2008*a*, *b*).

3. THE RELEVANT PARAMETERS

We first use the same parameters as in Shoucri and Afeyan (2014), for the study we are presenting here for the SRBS and SKEENS processes. A characteristic parameter by which to refer to the amplitude of laser field is the normalized vector potential or quiver momentum $|\vec{a}_\perp| = \left|e\vec{A}_\perp/M_e c\right| = a_0$, where $\vec{A}_\perp$ is the vector potential of the pump wave. For the linearly polarized wave, $a_0^2 = I\lambda_0^2/1.368 \times 10^{18}$. Here, I is the laser intensity in W/cm^2, and λ_0 the laser wavelength in microns. The pump wave frequency ω_{0P} of the injected laser beam is such that $\omega_{0P}/\omega_{pe} = 1/\sqrt{n/n_{cr}}$, where n_{cr} is the critical density for the pump. In our calculation, $n/n_{cr} = 0.0825$, which corresponds to a pump frequency $\omega_{0P} = 3.481$ (normalized to ω_{pe}). The amplitude of the vector potential of the pump is $a_{0P} = 0.025$. The seed backward pulse has a frequency $\omega_{0B} = 2.1657$. The amplitude of the vector potential of the seed pulse for the Raman scattered backward wave is $a_{0B} = a_{0P} = 0.025$. The parameters of the backward KEEN wave will be discussed in Section 3.1.

The frequency and wavenumber (ω_{0P}, k_{0P}) of the pump wave are related by the relation $\omega_{0P}^2 = \omega_{pe}^2 + k_{0P}^2 c^2$, or in normalized units $\omega_{0P}^2 = 1 + k_{0P}^2$, from which $k_{0P} = 3.3343$. For the stimulated Raman scattering, or the coupling of a pump light wave to a daughter scattered light wave and an EPW, the values of the electron plasma wavenumber k_{eB} associated with SRBS mode, and k_{eF} associated with the SRFS mode are

https://doi.org/10.1017/S0263034616000495 Published online by Cambridge University Press

roots of the equation (Bers *et al.*, 2009):

$$\left[\left(\frac{15\Omega}{4-6}\right)\right]K^4+(\mu+3\Omega-3)K^2-2\mu^{1/2}\left[\Omega^2-1+\left(\frac{5}{2\mu}\right)\right]^{1/2}K+2\Omega-1-\left(\frac{5}{2\mu}\right)(\Omega-1)=0 \tag{9}$$

with $K=k_e\lambda_{De}$, where λ_{De} is the Debye length. In our normalized units, the Debye length $\lambda_{De}=\upsilon_{te}/c=0.04424\sqrt{T_e}$ (λ_{De} normalized to c/ω_{pe} in our units, and T_e is in keV), and $\Omega=\omega_{0P}$ (normalized to ω_{pe}). For the present problem we use hydrogen ions with $M_i/M_e=1836$. We assume an electron temperature $T_e=2$ keV, so $\lambda_{De}=0.06256$. In Eq. (9), the parameter $\mu=m_ec^2/\kappa T_e=c^2/\upsilon_{te}^2=1/(0.04424\sqrt{T_e})^2=255.8$. The resulting roots are $k_{eB}\lambda_{De}=0.3377$ for the plasma mode associated with the SRBS, and $k_{eF}\lambda_{De}=0.0666$ for the plasma mode associated with the SRFS. As discussed in Bers *et al.* (2009), for these parameters the SRBS plasma wave is damped, and the damping of the SRFS plasma wave is small. The heavily damped regime with $k_e\lambda_{De}>0.29$ is called the kinetic regime (Shoucri & Afeyan, 2014). We finally get $k_{eB}=0.3377/\lambda_{De}=5.398$ for the SRBS plasma wave, and $k_{eF}=0.0666/\lambda_{De}=1.0645$ for the SRFS plasma wave. The corresponding frequencies for the SRBS plasma wave and the SRFS plasma wave are solutions of the equation (Bers *et al.*, 2009):

$$\omega^2\approx 1+3k^2\lambda_{De}^2/\omega^2+15k^4\lambda_{De}^4/\omega^4-5/(2\mu). \tag{10}$$

We get from Eq. (10) for the SRBS wave $\omega_{eB}=1.178$, and for the SRFS plasma wave $\omega_{eF}=1.0066$. The selection rules give the following results for the forward scattered electromagnetic wave (ω_{0F}, k_{0F}) and the backward scattered electromagnetic wave (ω_{0B}, k_{0B}):

$$\begin{aligned}\omega_{0B}&=\omega_{0P}-\omega_{eB}=3.481-1.178=2.303;\\ \omega_{0F}&=\omega_{0P}-\omega_{eF}=3.481-1.0066=2.4744;\end{aligned} \tag{11}$$

$$\begin{aligned}k_{0B}&=k_{eB}-k_{0P}=5.398-3.3343=2.0637;\\ k_{0F}&=k_{0P}-k_{eF}=3.3343-1.0645=2.2698.\end{aligned} \tag{12}$$

Note the close values of (ω_{0F}, k_{0F}) with (ω_{0B}, k_{0B}). We verify that the results in Eqs. (11) and (12) obey the dispersion relation of the electromagnetic wave $1+k_{0F}^2=\omega_{0F}^2$ (from which we get $\omega_{0F}=2.48$), and $1+k_{0B}^2=\omega_{0B}^2$ (from which we get $\omega_{0B}=2.293$). These results are in very good agreement with the results calculated in Eq. (11). We note also the possibility of the anti-Stokes resonance $\omega_{as}=\omega_{0P}+\omega_{eF}=3.481+1.006=4.487$, $k_{as}=k_{0P}+k_{eF}=3.3343+1.0645=4.399$. We calculate from the relation $1+k_{as}^2=\omega_{as}^2$ a value $\omega_{as}=4.511$, close to the value of 4.487 calculated from the selection rule. In addition, KEEN waves have been identified in (Afeyan *et al.* 2004, 2014, Mehrenberger *et al.* 2013, Shoucri and Afeyan 2014), which do not belong to the dispersion relations presented in Eqs. (9) and (10). The KEEN waves resulted from the scattering of the pump with the backward stimulated wave at (ω_{0F}, $-k_{0F}$), where (ω_{0F}, k_{0F}) are the frequency and wavenumber of the SFRS wave calculated in Eqs. (9) and (10). These will be discussed in more details in Section 3.1.

The ions were included in the calculation, but did not play any role in the physics except establishing a small self-consistent sheath at the edges. We use a fine resolution grid in phase space, with $N=30{,}000$ grid points in space, and 512 grid points in momentum space for the electrons (extrema of the electron momentum are ± 0.5). We have initially a flat profile of a uniform plasma slab with the normalized density $n_e=n_i=1$. This flat profile of the uniform plasma extends over a length $L_p=570.8c/\omega_{pe}$. On either side of the initial plasma slab the densities are smoothly brought down to zero through an initial parabolic profile of length $L_{edge}=8c/\omega_{pe}$. An extra vacuum region of length $L_{vac}=6.6c/\omega_{pe}$ exists on each side of the slab, for a total length of the system of $L=600c/\omega_{pe}$. In our normalized units $\Delta x=\Delta t=0.02$. We also have $\Delta x/\lambda_{De}=0.02/0.0626\approx 0.32$.

3.1. Stimulated KEEN Wave Backscattering Pulse

The forward propagating linearly polarized wave is injected in the domain at the left boundary at $x=0$ with $E^+=2E_{0P}\cos(\omega_{0P}t)$, $E_{0P}=\omega_{0P}a_{0P}$, with $a_{0P}=0.025$. The pump precursor reaches the right boundary at $t=600$ (since in our normalized units $x=t$). As will be explained below, the KEEN wave is excited when a backward seed pulse is injected at the frequency of the forward scattered mode $\omega_{0F}=2.474$ (Shoucri & Afeyan, 2014). A seed pulse is injected at $x=L$ in the backward direction in the form $E^-=-2E_{0K}P_{0K}(t)\cos\omega_{0F}\tau$, where $\tau=t-t_1$. The temporal shape factor of the seed pulse is $P_{0K}(t)=\exp(-0.5(t-t_0)^2/\tau_s^2)$, for $t_1<t<t_2$. In this simulation we have $\tau_s=15$, $t_0=550$, $t_2=600$, $t_1=500$, and $E_{0K}=\omega_{0F}a_{0K}$, with $a_{0K}=a_{0P}$. In this way, the seed Gaussian pulse starts penetrating the domain from the right boundary at $t=t_1=500$. When the pump precursor has reached the right boundary $x=L=600$ at $t=600$, the seed pulse injected at the right boundary of the domain in the backward direction has fully penetrated from the right boundary, and its peak has reached the point at $x=550$ at the time $t=600$.

We present first the results obtained for the forward propagating wave before the injection of the pulse. We show in Figure 1 the wavenumber spectra of the forward propagating signal E^+, the backward propagating signal E^-, and the longitudinal electric field. E^+ and E^- are defined in Eq. (3). These spectra are calculated in the domain $x=(20,164)$, at $t=800$, well before the arrival of the seed pulse injected from the right boundary. The spectrum of E^+ shows the peak of the pump at $k_{0P}=3.3364$, the peak of the forward scattered mode $k_{0F}=2.2626$, very close to the value

https://doi.org/10.1017/S0263034616000495 Published online by Cambridge University Press

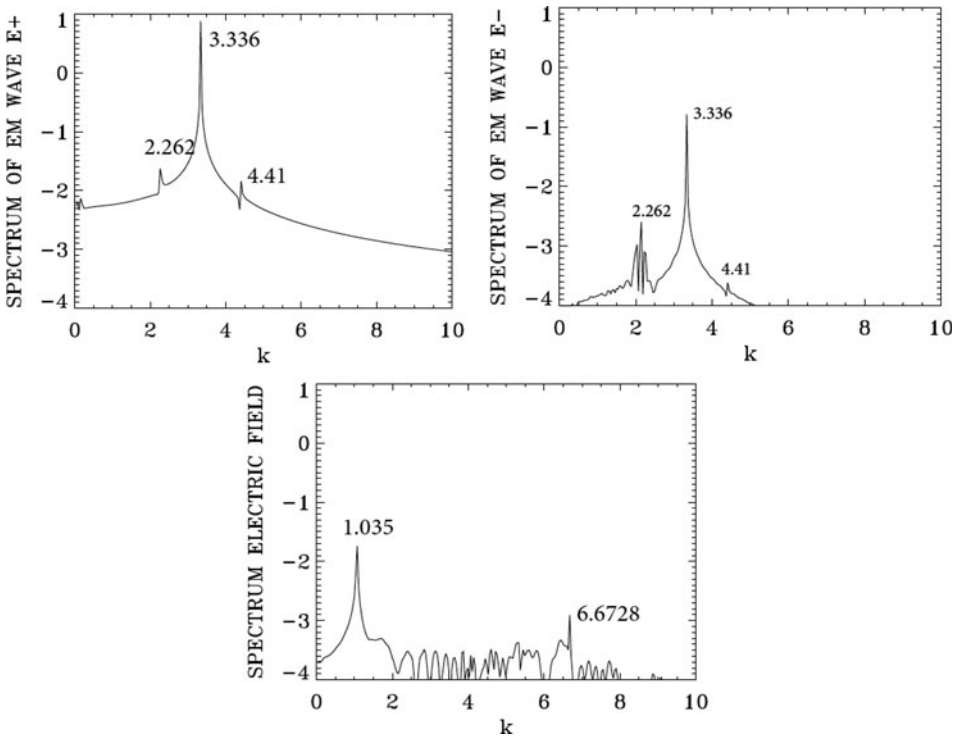

Fig. 1. Wavenumber spectra of (clockwise) the incident wave E^+, the backward wave E^-, and the longitudinal electric field E_x, in the domain $x = (20,164)$ at $t = 800$.

calculated in Eq. (12), and a small peak of the anti-Stokes mode at $k_{as} = 4.41$, very close to the theoretical value calculated at 4.399.

In free space, the forward propagating wave E^+ and the backward propagating wave E^- are strictly decoupled. In a plasma, there is a very weak coupling between E^+ and E^- due to the nonlinearity of the medium. So the wavenumber spectrum of the backward wave E^- in the same domain $x = (20,164)$ in Figure 1 shows the same peaks at 2.262, 3.336, and 4.41, but at a much lower level, even though the injected seed pulse at the right still did not reach the domain $x = (20,164)$. Finally, we present also in Figure 1 the spectrum of the longitudinal electric field, which shows a broad peak at $k_{eF} = 1.035$ [theoretical value of 1.064 calculated from Eq. (9)]. We also see the peak at 6.6728.

Indeed, for the linearly polarized wave, we have a plasma mode appearing at the harmonic of the pump $2k_{0P} = 6.6728$. This is due to the fact that if we have a linearly polarized wave: $\vec{E} = (0, E_y, 0)$, we can write in a linear analysis with $E_y = E_0 \cos(\psi)$, $\psi = (kx - \omega t)$, using Faraday's law:

$$\frac{\partial \vec{B}}{\partial t} = \left(0, 0, -\frac{\partial E_y}{\partial x}\right). \tag{13}$$

Then $\vec{B} = (0, 0, B_z)$ with $B_z = B_0 \cos(\psi)$, and $B_0 = E_0 k/\omega$. From $\vec{E}_\perp = -\partial \vec{a}_\perp/\partial t$ from Eq. (2), and $\vec{p}_\perp = \vec{a}_\perp$, we get $\vec{p} = (0, p_y, 0)$, with $p_y = -p_0 \sin(\psi)$, and $p_0 = E_0/\omega$. The longitudinal Lorentz force is $p_y B_z = -(1/2) k p_0^2 \sin(2\psi)$. This drives a longitudinal response at the harmonic of the laser wave.

Figure 2 presents the frequency spectra of the waves. The frequency spectrum of the forward wave E^+ presented in Figure 2 shows the peak of the pump wave at $\omega_{0P} = 3.4898$ (calculated at 3.481 in our theoretical results), the forward scattered frequency at $\omega_{0F} = 2.474$, as calculated in Eq. (11), and the frequency of the anti-Stokes mode at $\omega_{as} = 4.51$ as calculated in our theoretical results above. As explained above, there is a weak coupling of E^+ and E^- which produces in the spectrum of E^- the same frequencies as for E^+, but at a much lower level.

The frequency spectrum of the longitudinal electric field shows a peak of the plasma wave resonant with the forward scattering of the pump at $\omega_{eF} = 1.00$ (theoretical value calculated at 1.0066). It also shows a peak at 6.96, which is the forced oscillation at the harmonic of the pump, as explained in Eq. (13). The small peaks at 5.963 and 7.976 seem to result from the resonance of the peak at 1.00 and the forced oscillation at 6.96, with 1.00 + 5.963 = 6.963 and 1.00 + 6.960 = 7.96.

As we mentioned above, there is a weak coupling of E^+ and E^- which produces in the spectrum of E^- a weak backward component at $(\omega_{0F}, -k_{0F})$. This backward wave can couple with the forward propagating pump to produce a KEEN wave with the selection rule coupling $k_{0p} = -k_{0F} + k_{keen}$, from which $k_{keen} = k_{0P} + k_{0F} = 3.334 + 2.27 = 5.60$, as calculated in Shoucri and Afeyan (2014). The frequency of this KEEN wave obey the coupling relation $\omega_{0P} = \omega_{0F} + \omega_{keen}$, from which $\omega_{keen} = 3.481 - 2.474 = 1.007$. The

https://doi.org/10.1017/S0263034616000495 Published online by Cambridge University Press

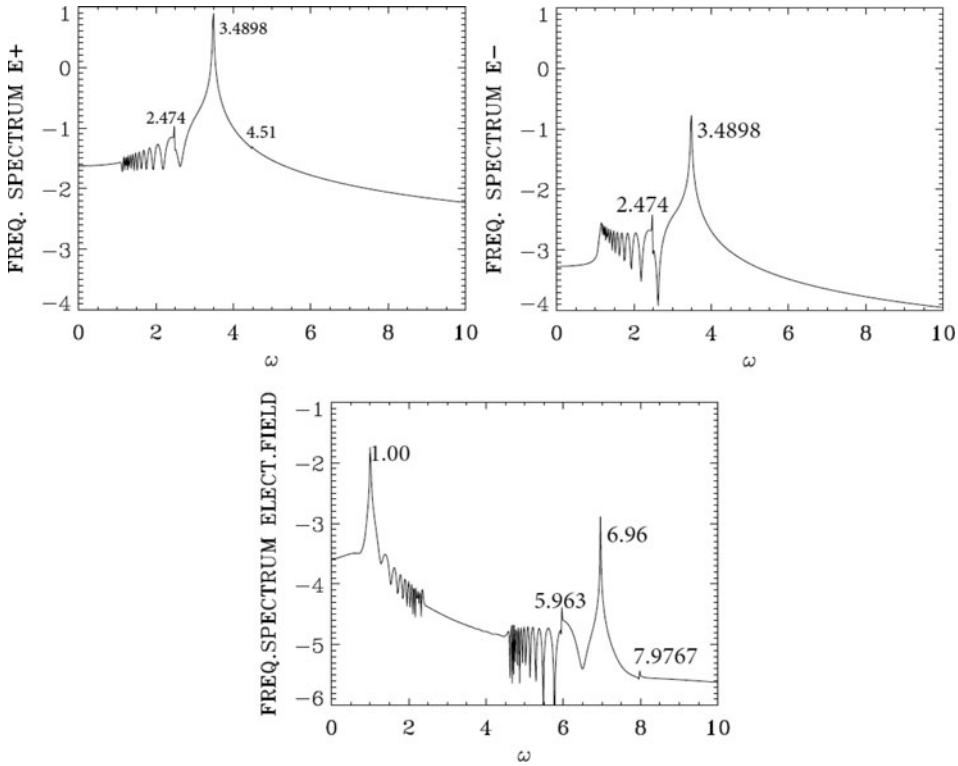

Fig. 2. Frequency spectra of (clockwise) the incident wave E^+, the backward wave E^-, and the longitudinal electric field E_x, at the position $x = 250$, at time $t = (260,328)$.

mode at 1.00 is indeed present in the spectrum of the longitudinal electric field in Figure 2 due to the forward Raman scattering, but the coupling with the KEEN wave at $-k_{0F}$ is weak and shows no response at the wavenumber k_{keen} in the spectrum of the longitudinal electric field, because the mode at $-k_{0F}$ in the spectrum of E^- in Figure 1 is very weak. In the results presented in Shoucri and Afeyan (2014), this mode was stimulated by a backward wave injected at $-k_{0F}$. This mode can also be stimulated in the present simulation by the pulse we injected as described above at the right boundary with a frequency ω_{0F}, propagating in the backward direction. We present in Figure 3 the electron density profile and the longitudinal electric field profile at $t =$ 840, when the pulse injected at the right boundary with a frequency ω_{0F} and traveling to the left has reached a point close to $x = 300$.

We present in Figure 4 the spectra of the longitudinal electric field at the arrival of this pulse (ω_{0F}, $-k_{0F}$) in the domain $x = (20,348)$, at $t = 800$ and at $t = 840$. We can verify from Figure 3 that at this time the signal has just penetrated from the right into the domain $x = (20,348)$. In Figure 4 at $t =$ 800 (left panel) we see indeed the growing mode (compare with Fig. 1) with a broad peak at $k_{keen} = 5.58$, very close to the theoretical value of 5.60 calculated in the previous paragraph. So the wavenumber response of the system to the backward pulse injected at the right boundary at the frequency ω_{0F} is indeed a KEEN wave at $k_{keen} = 5.58$. The right panel in Figure 4 gives the wavenumber spectrum at $t = 840$

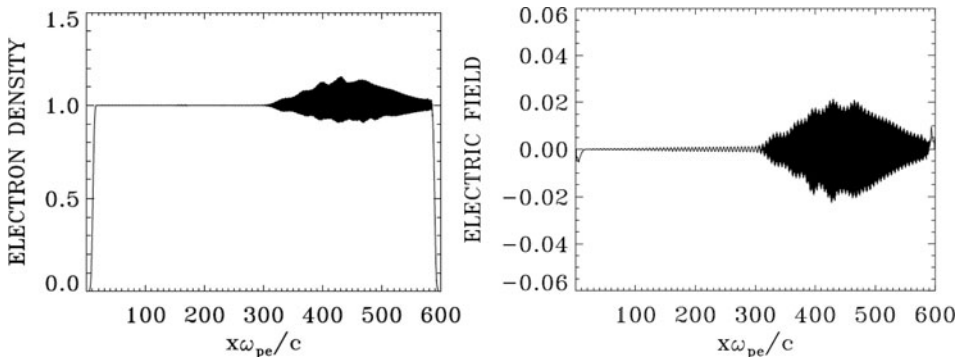

Fig. 3. Plot of the electron density profile (left frame) and the longitudinal electric field E_x (right frame) at time $t = 840$.

https://doi.org/10.1017/S0263034616000495 Published online by Cambridge University Press

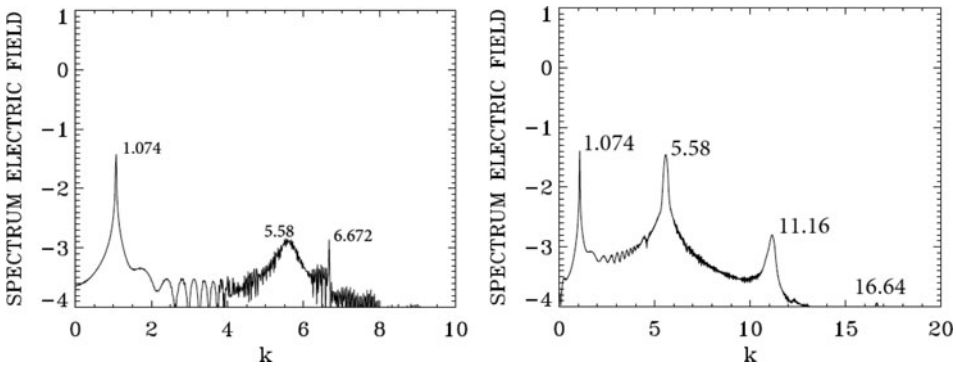

Fig. 4. Wavenumber spectra of the longitudinal electric field E_x in the domain $x = (20,348)$, at time $t = 800$ (left frame), and $t = 840$ (right frame).

in the same domain, showing again the continued growth of the mode at $k_{\text{keen}} = 5.58$, which is now developing a harmonic structure.

We present in Figure 5 the wavenumber spectra of the forward wave E^+ and backward wave E^- at $t = 840$. The presence of the backward mode k_{0F} at 2.262 in the spectrum of E^- is now growing to become dominant, showing a broad peak. So the system is responding to the arrival of the seed pulse injected with $\omega_{0F} = 2.474$ from the right boundary in the backward direction with a growing mode at $k_{0F} = 2.262$ in the spectrum of E^- as it should. The forward wave E^+ at $k_{0P} = 3.336$ can now couple with the backward wave of the pulse at $-k_{0F} = -2.262$ with $k_{0p} = -k_{0F} + k_{\text{keen}}$ to produce the KEEN wave with $k_{\text{keen}} = k_{0P} + k_{0F} = 3.334 + 2.262 = 5.596$, which we observe at 5.58 in Figure 4. The wavenumber at $k_{eF} = 1.074$ in Figure 4 is the result of the forward scattering $k_{0P} = k_{0F} + k_{eF}$, calculated at $k_{eF} = 1.0645$ in our theoretical results in Eq. (12).

The frequency spectra are presented in Figure 6. These spectra are calculated from the registered signals at $x = 250$ at the arrival of the pulse, from the time $t = 623$ to $t = 990$. We see in the spectrum of the forward wave E^+ the presence of the pump frequency at $\omega_{0P} = 3.4898$, of the forward scattered mode at $\omega_{0F} = 2.474$, and the anti-Stokes mode $\omega_{as} = 4.49$. The frequency spectrum of the backward wave E^- shows the peak at 3.4898, and a broad peak at 2.454 (slightly shifted from the value of 2.474 observed in Fig. 2). The coupling of forward wave E^+ at 3.4898 and the backward wave at 2.454 according to the selection rule $\omega_{0P} = \omega_{0F} + \omega_{\text{keen}}$ produces the frequency $3.4898 - 2.454 = 1.036$, very close to the value of 1.054 in the broad peak appearing the spectrum of the longitudinal electric field in Figure 6. We note also in the spectrum of the longitudinal electric field in Figure 6 the values of 1.00, and 6.96 previously identified in Figure 2. Different small peaks are also appearing. It is important at this stage to insist on the transient nature of the modes we are studying.

We present in Figure 7 a phase-space plot at $t = 840$ showing the growth of the KEEN wave at the arrival of the backward pulse around $x = 320$. The phase velocity of the KEEN wave is $\upsilon_{\text{keen}} = 1.054/5.58 = 0.19$, corresponding to $p_{\text{keen}} = \upsilon_{\text{keen}}/\sqrt{1 - \upsilon_{\text{keen}}^2} = 0.1935$, which is essentially the value we see at the center of the vortex at the right in Figure 7.

After the analysis we have presented of the initial KEEN response of the system to the pulse injected at the right boundary at the frequency $\omega_{0F} = 2.474$, we now look to the final evolution of the system. We present in Figure 8 a plot at $t =$ 1000 and 1116 of the incident pump (full curve) and the pulse (dashed curve). The pulse injected at the right boundary in the backward direction as explained before has now traveled to the left. The incident pump with constant

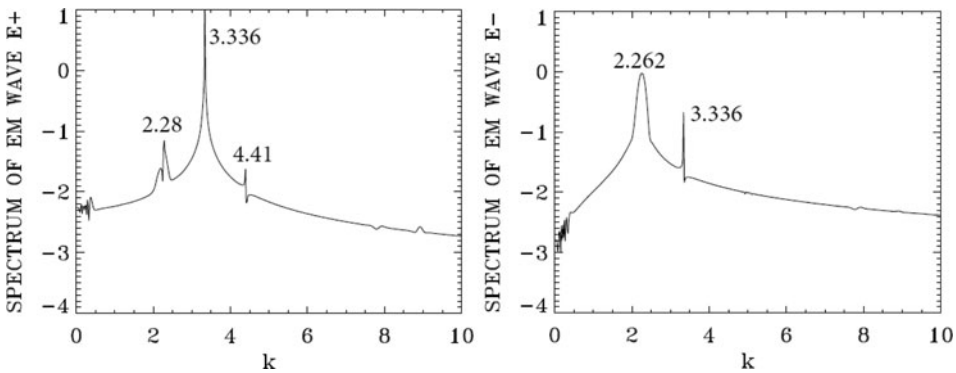

Fig. 5. Wavenumber spectra of the forward pump wave E^+ (left frame) and the backward wave E^- (right frame), in the domain $x = (20,348)$ at $t = 840$.

https://doi.org/10.1017/S0263034616000495 Published online by Cambridge University Press

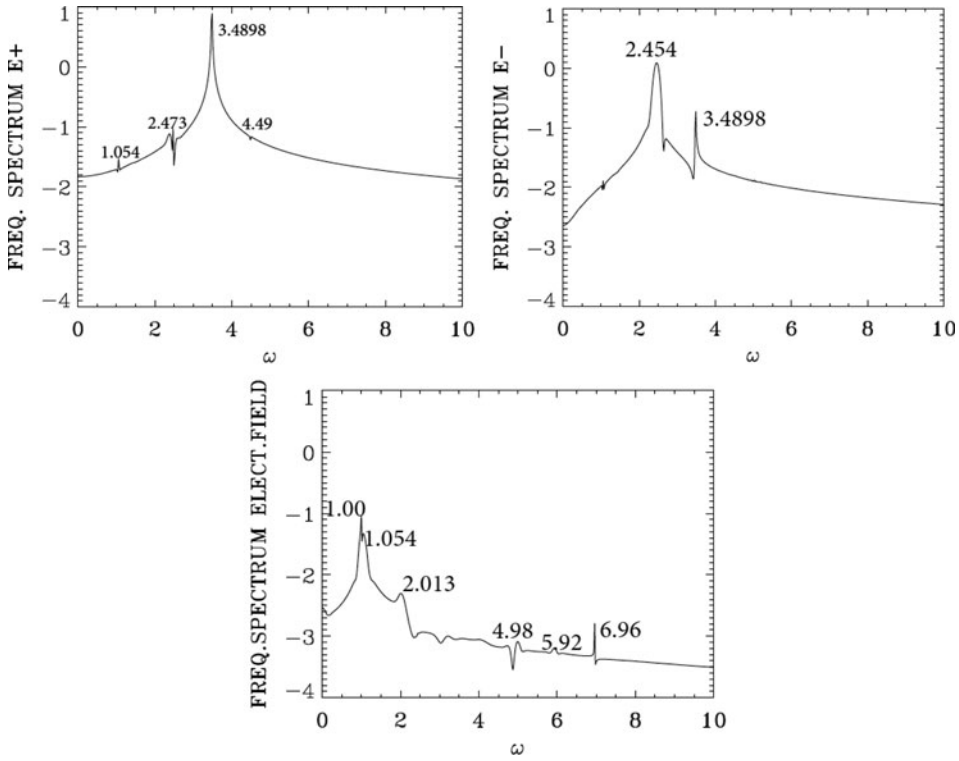

Fig. 6. Frequency spectra of (clockwise) the incident wave E^+, the backward wave E^-, and the longitudinal electric field E_x, at the position $x = 250$, at time $t = (623{,}990)$.

amplitude at the left boundary goes through a phase of partial depletion after the crossing of the pulse coming from the right. The growth of the pulse is small in the present case, and does not show a significant contraction. Its initial peak value of E^- when injected was $2\omega_{0F}a_{0K} = 0.124$, and is reaching toward the end (see the dashed curve in Fig. 8) a value about 0.4, more than three times higher than the initially injected amplitude, and about twice bigger than the amplitude of the injected pump E^+ field at the left.

Figure 9 presents the plot of the electron density and the longitudinal electric field at $t = 1000$. It shows the profile maintaining a coherent structure.

Figure 10 presents the wavenumber spectra of the pump E^+, the backward wave E^-, and the longitudinal electric field, taken in $x = (180{,}344)$ at $t = 1000$, at the edge where from Figure 9 the spatial structure appears coherent. We see the now dominant peak of the backward wave E^- at 2.186. The peak of the pump E^+ appears at $k_{0p} = 3.336$.

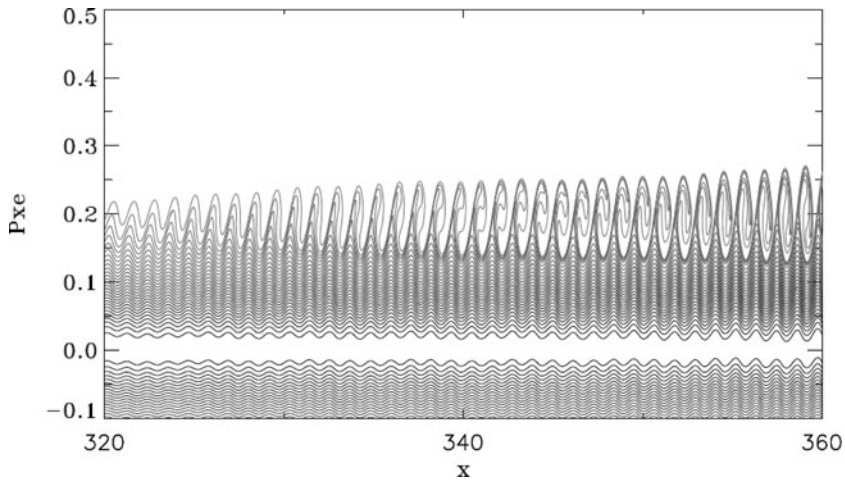

Fig. 7. Phase-space plot of the electron distribution function in the domain $x = (320{,}360)$, at time $t = 840$ at the arrival of the KEEN wave around $x = 320$.

https://doi.org/10.1017/S0263034616000495 Published online by Cambridge University Press

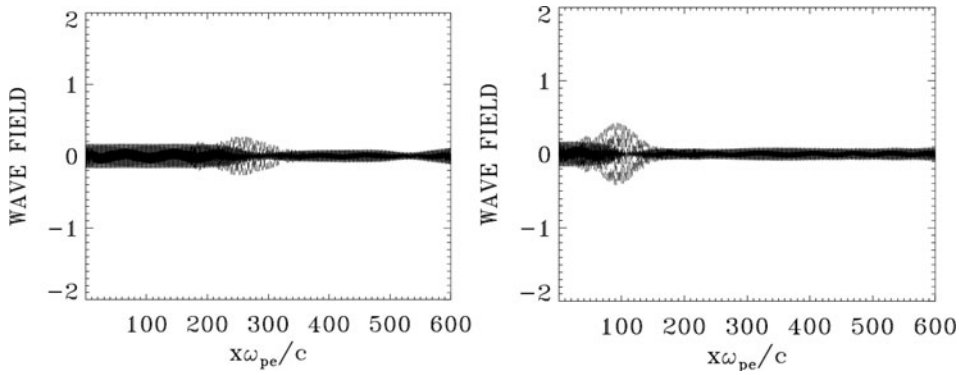

Fig. 8. The evolution of the incident forward pump wave E^+ (full curve), and the backward seed pulse E^- (dashed curve) at $t = 1000$ (left frame) and $t = 1116$ (right frame).

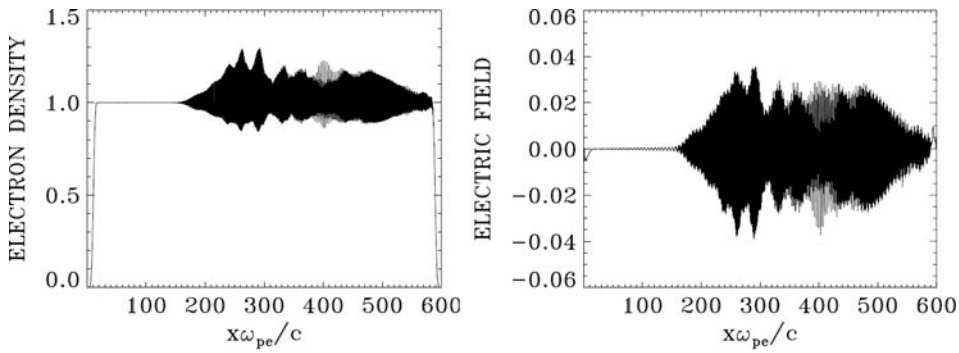

Fig. 9. Plot of the electron density profile (left frame) and the longitudinal electric field E_x (right frame) at time $t = 1000$.

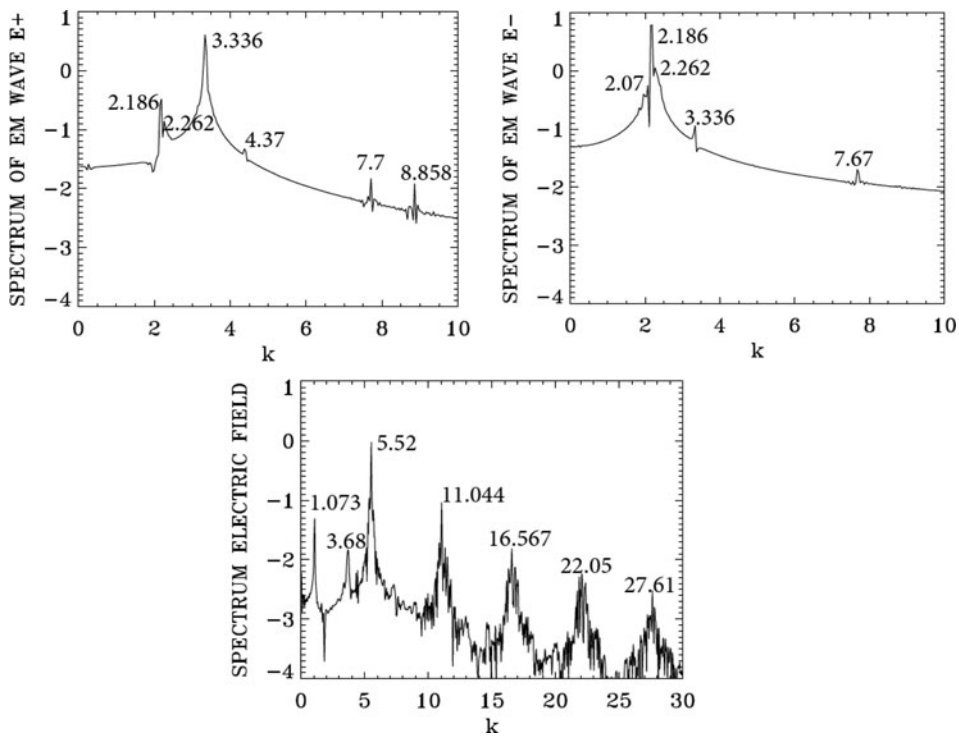

Fig. 10. Wavenumber spectra of (clockwise) the incident wave E^+, the backward wave E^-, and the longitudinal electric field E_x, in the domain $x = (180,344)$ at $t = 1000$.

https://doi.org/10.1017/S0263034616000495 Published online by Cambridge University Press

We still have a forward scattering, and the forward scattered mode appears now at $k_{0F} = 2.262$, previously obtained in Figures 1 and 5. The plasma mode k_{eF} resulting from the forward scattering $k_{0p} = k_{0F} + k_{eF}$ is present in the spectrum of the longitudinal electric field at $k_{eF} = 3.336 - 2.262 = 1.074$. The wavenumber of the KEEN wave is now determined by the pump interacting with the backward dominant peak at 2.186, at $k_{keen} = 3.336 + 2.186 = 5.522$, clearly dominant in the spectrum of the longitudinal electric field in Figure 10 (slightly shifted from the value of 5.58 initially calculated in Fig. 4). We see also the harmonic of this peak appearing in the wavenumber spectrum of the longitudinal electric field in Figure 10. We note in the spectrum of E^+ the peak of the anti-Stoke at 4.37. We now also see the small peak of the backward Raman scattered mode appearing at $k_{0B} = 2.07$ in the spectrum of E^- [calculated at 2.0637 in Eq. (12)]. The now dominant backward mode at 2.186 in the spectrum of E^- can also directly interact with the plasma KEEN mode, generating the mode at −7.67, with the relation $-2.186 = -7.67 + k_{keen}$, from which we get $k_{keen} = 5.484$ (appearing at 5.522 in the spectrum in Fig. 10). And in the spectrum of E^+ the pump at 3.336 can also directly interact with the plasma KEEN mode, generating the mode at 8.858, with the relation $8.858 = 3.336 + k_{keen}$, from which we get $k_{keen} = 5.522$, appearing in the spectrum in Figure 10. Also in the spectrum of E^+ the mode 7.7 couples with the mode at 2.186 through the relation $7.7 = 2.186 + k_{keen}$, from which $k_{keen} = 5.514$, very close to the value of 5.52 in Figure 10.

The frequency spectra registered at time $t = (920,1084)$, during the passage of the homogeneous front of the signal at the point $x = 250$, are presented in Figure 11. The spectrum of the pump E^+ shows the frequency $\omega_{0P} = 3.4898$, the backward wave E^- is now dominated by a broad peak at the frequency 2.377 (evolving by a small shift from the value of 2.474 in Fig. 2 and 2.454 in Fig. 6). The relation $3.4898 = 2.377 + \omega_{keen}$ gives $\omega_{keen} = 1.11$, close to the broad peak at 1.073 in the frequency spectrum of the longitudinal electric field in Figure 11. The frequency of the anti-Stoke is at 4.487.

We present in Figure 12 the plots of the electron density and the longitudinal electric field at the end of the simulation at $t = 1116$. The front edge is still maintaining coherence, and hence still maintaining the growth of the pulse, while the remaining profile is becoming chaotic due to the fusion of vortices in the phase space. The vortices in the front edge are presented in Figure 13, in $x = (20,60)$ and $x = (60,100)$. We present in Figure 14 the distribution function spatially averaged over a wavelength at $t = 1116$, taken from the results in Figure 13, at the position $x = 60$ and 100.

Figure 15 presents the wavenumber spectra of the pump E^+, the backward wave E^-, and the longitudinal electric field, taken at the front edge in $x = (20,102)$ at $t = 1116$, at the end of the simulation. They are close to what is presented

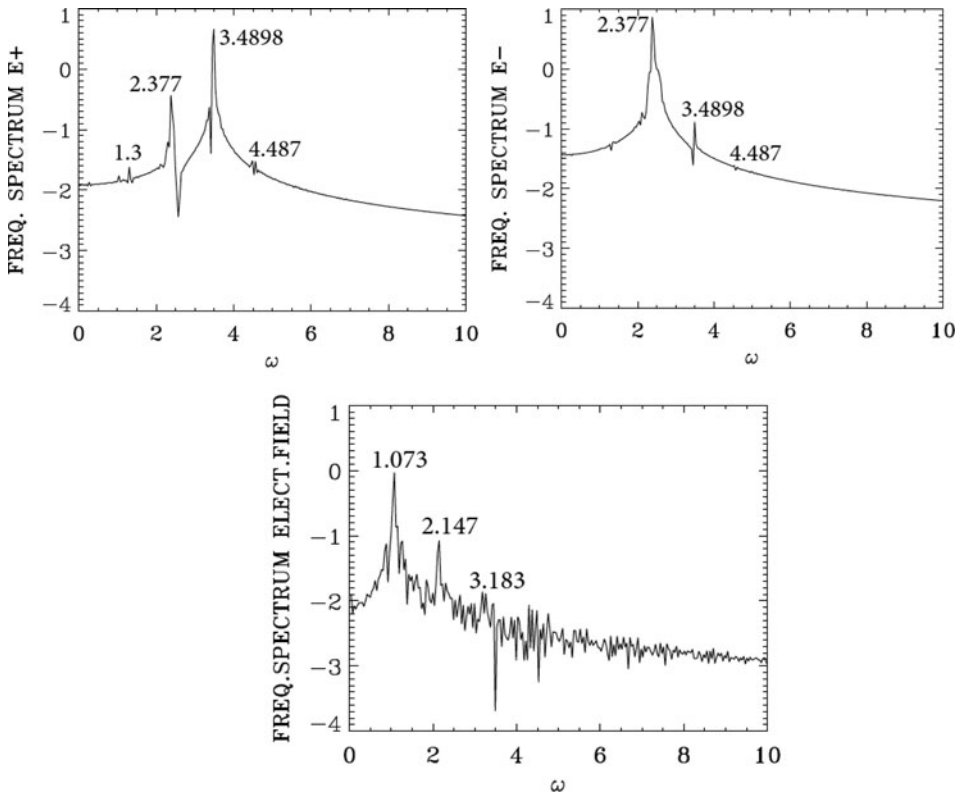

Fig. 11. Frequency spectra of (clockwise) the incident wave E^+, the backward wave E^-, and the longitudinal electric field E_x, at the position $x = 250$, at time $t = (920,1084)$.

https://doi.org/10.1017/S0263034616000495 Published online by Cambridge University Press

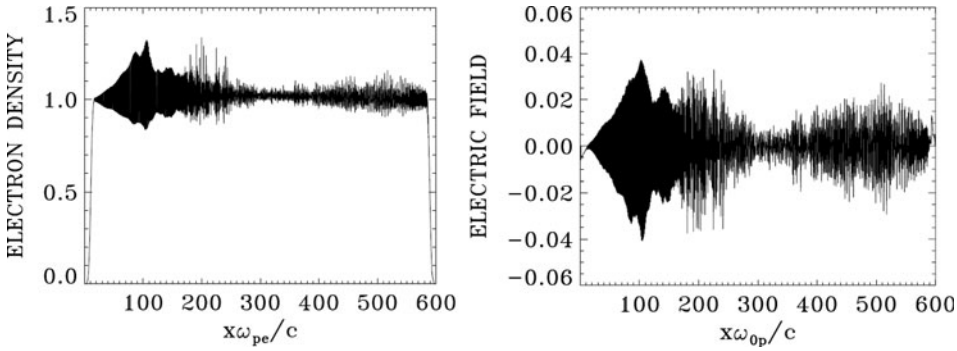

Fig. 12. Plot of the electron density profile (left frame) and the longitudinal electric field E_x (right frame) at time $t = 1116$.

in Figure 10. We see the now dominant peak of the backward wave E^- at 2.186. The peak of the pump E^+ appears at $k_{0p} = 3.374$. We still have a forward scattering, and the forward scattered mode appears now at $k_{0F} = 2.3$, slightly shifted from the value of 2.262 obtained in Figures 1 and 5, since the plasma mode k_{eF} resulting from the forward scattering $k_{0P} = k_{0F} + k_{eF}$ is present in the spectrum of the longitudinal electric field at $k_{eF} = 3.374 - 2.3 = 1.074$. The wavenumber of the KEEN wave is now determined by the pump interacting with the backward dominant peak at 2.186, at $k_{keen} = 3.374 + 2.186 = 5.56$, very close to the peak calculated at 5.522 in Figure 15 (slightly shifted from the value of 5.58 in Fig. 4). We see also the harmonic of this peak appearing in the wavenumber spectrum of the longitudinal electric field in Figure 15. We note in the spectrum of E^+ the peak of the anti-Stoke at 4.41. We now see also a small peak of the backward Raman scattered mode appearing at $k_{0B} = 2.07$ in the spectrum of E^- [calculated at 2.0637 in Eq. (12)]. The now dominant backward mode at 2.186 can also directly interact with the plasma KEEN mode, generating in the backward direction the mode at 7.746 in the spectrum of E^-, with the relation $-2.186 = -7.746 + k_{keen}$, from which we get $k_{keen} = 5.56$ (appearing at 5.522 in the spectrum).

The frequency spectra registered in $t = (920,1084)$, during the passage of the homogeneous front of the signal at the point $x = 250$, are presented in Figure 11.

3.2. Raman Backscattered Wave Pulse

We use the same parameters as in Section 3.1. However, the pulse injected at the right boundary has a frequency $\omega_{0B} = 2.30$, which is the frequency of the backward scattered Raman wave, which is calculated in Eq. (11). The pump and all other parameters remain the same. The first part of the simulation, when the pump is propagating in the forward direction, before the injection of the pulse, is therefore identical to what has been presented in Figures 1 and 2 for the excitation of the Raman forward scattered wave. After the injection of the pulse from the right boundary in the backward direction in the same way as described above for the KEEN wave, the propagating pulse will interact with the pump and start growing. Figure 16 shows the density plot and the electric field plot at $t = 840$, to be compared with Figure 3. There is a difference in the spatial topology of these plots, compared with the corresponding ones in Figure 3.

Figure 17 shows the wavenumber spectra of the longitudinal electric field at $t = 800$ (left panel) and $t = 840$ (right panel), at the time the pulse injected from the right boundary is arriving in the domain $x = (20,348)$, to be compared with Figure 4. We see in the left panel the system responding with the appearance of the plasma wave at $k_{eB} = 5.39$ due to the backward Raman scattering in agreement with Eq. (12), in addition with the plasma wave at $k_{eF} = 1.074$ due to the forward Raman scattering [calculated at 1.0645 in Eq. (12)], and

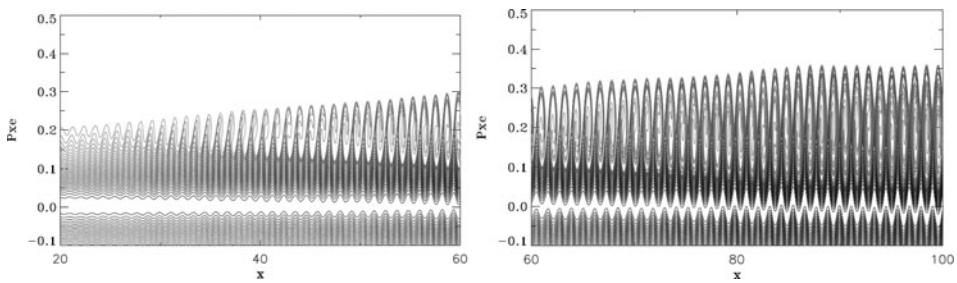

Fig. 13. Phase-space plot of the electron distribution function in the domain $x = (20,100)$, showing the vortices in the front edge at time $t = 1116$.

https://doi.org/10.1017/S0263034616000495 Published online by Cambridge University Press

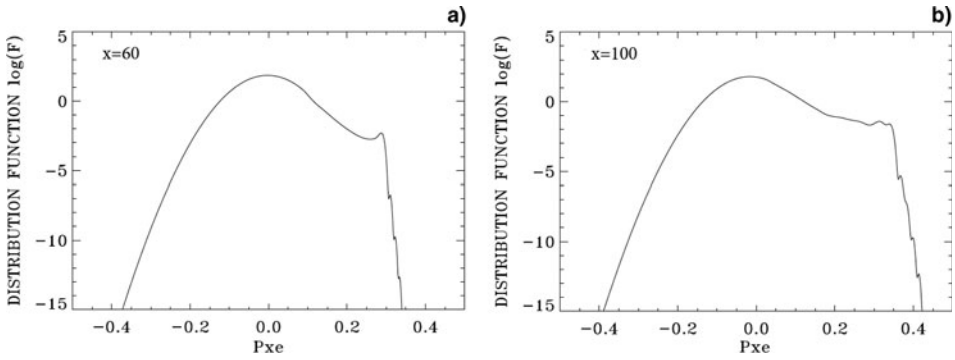

Fig. 14. The distribution function spatially averaged over a wavelength around the positions (a) $x = 60$ and (b) $x = 100$, at time $t = 1116$.

the mode at the pump harmonic $2k_{0P} = 6.672$, as explained in the previous section at Eq. (13).

The right panel in Figure 17 shows the spectrum of the electric field at $t = 840$. The plasma mode is slightly shifted at $k_{eB} = 5.426$, and has developed harmonics at 10.872 and 16.413. The wavenumber spectra of the forward pump wave E^+ and the backward wave E^- at $t = 840$ are presented in Figure 18. We see in addition to what is presented in Figure 5, the appearance of the backward pulse with wavenumber at 2.07 [calculated at 2.063 in Eq. (12)], which is now the dominant mode in the spectrum of the backward wave E^-. To be compared with Figure 5.

The frequency spectra of the growing waves at the arrival of the pulse are calculated from the recorded signal at $x = 250$ from $t_1 = 623$ to $t_2 = 951$. In Figure 19, we present the frequency spectra of the forward pump wave E^+, the backward pulse wave E^- and the longitudinal electric field. We see in the spectrum of E^- the dominant backward pulse wave at the frequency 2.32 [calculated at 2.30 in Eq. (11)]. This peak appears in the spectrum of E^+, together with the frequency of the forward scattered mode at 2.474, the pump frequency at 3.4898, and the anti-Stoke frequency at 4.48. The frequency spectrum of the evolving longitudinal wave in Figure 19 show a broad peak at 1.16, and the frequency at the harmonic of the pump frequency $2\omega_{0P} = 6.96$, as explained in Eq. (13). Figure 19 is to be compared with Figure 6.

We present in Figure 20 a phase-space plot at $t = 840$ showing the growth of the backward Raman scattered wave

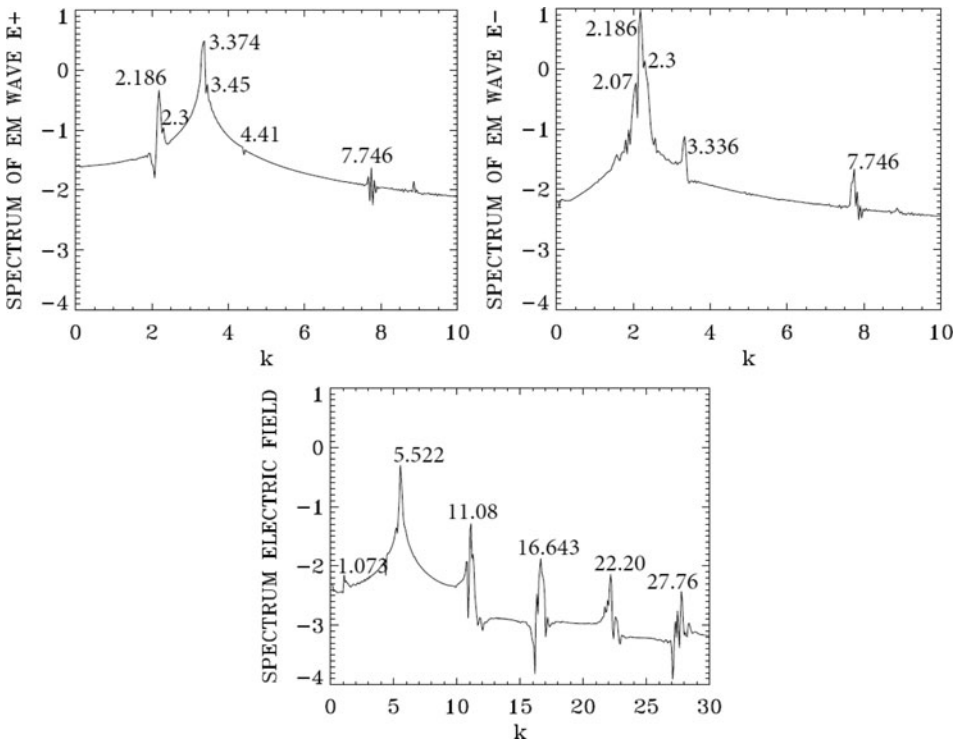

Fig. 15. Wavenumber spectra of (clockwise) the incident wave E^+, the backward wave E^-, and the longitudinal electric field E_x, in the domain $x = (20,102)$ at $t = 1116$.

https://doi.org/10.1017/S0263034616000495 Published online by Cambridge University Press

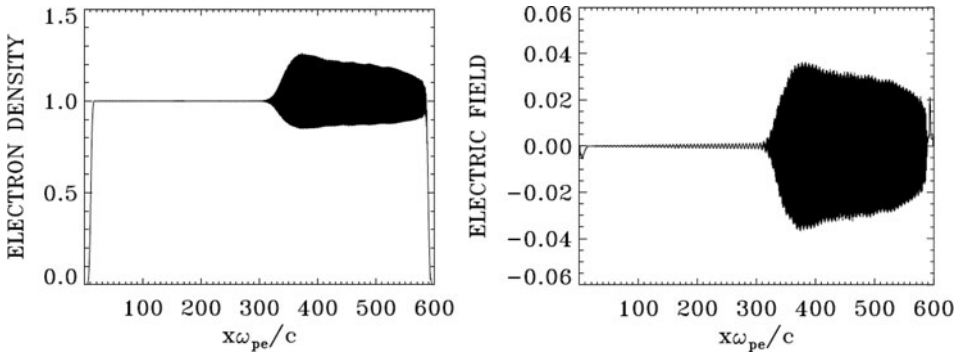

Fig. 16. Plot of the electron density profile (left frame) and the longitudinal electric field E_x (right frame) at time $t = 840$.

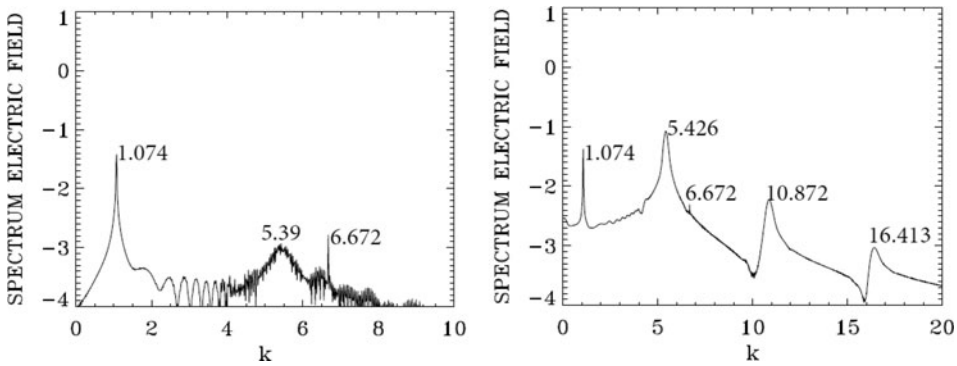

Fig. 17. Wavenumber spectra of the longitudinal electric field E_x in the domain $x = (20,348)$, at time $t = 800$ (left frame), and $t = 840$ (right frame).

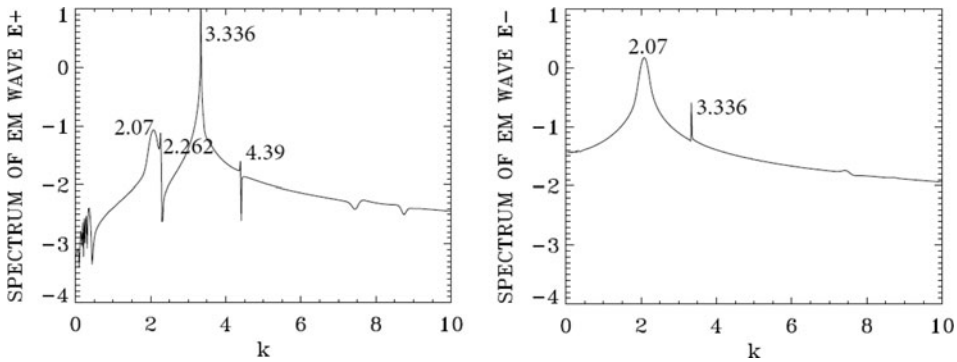

Fig. 18. Wavenumber spectra of the forward pump wave E^+ (left frame) and the backward wave E^- (right frame), in the domain $x = (20,348)$ at $t = 840$.

at the arrival of the backward pulse around $x = 320$, showing a much more rapid growth compared with Figure 7.

The density and longitudinal electric field plots at $t = 1000$ are shown in Figure 21. They are still maintaining the coherent structure. However, the morphology of the modulations in Figure 21 are sharply different from what we observed in Figure 9. Figure 22 presents the plots of the forward pump wave E^+ (full curve) and the backward pulse wave E^- (dashed curve) at $t = 1000$ (left panel) and $t = 1116$ (right panel). The growth of the pulse is more important to what is presented in Figure 8.

We present now the final state of the system. Figure 23 presents the plot of the density and the longitudinal electric field at $t = 1116$. It shows the front maintaining a coherent structure, while to the right the fusion of the excited vortices is creating a chaotic structure. We look in Figure 24 into the phase space of the coherent structure at the left in Figure 23, from $x = 20$ to 100. It shows a dominant vortex structure.

https://doi.org/10.1017/S0263034616000495 Published online by Cambridge University Press

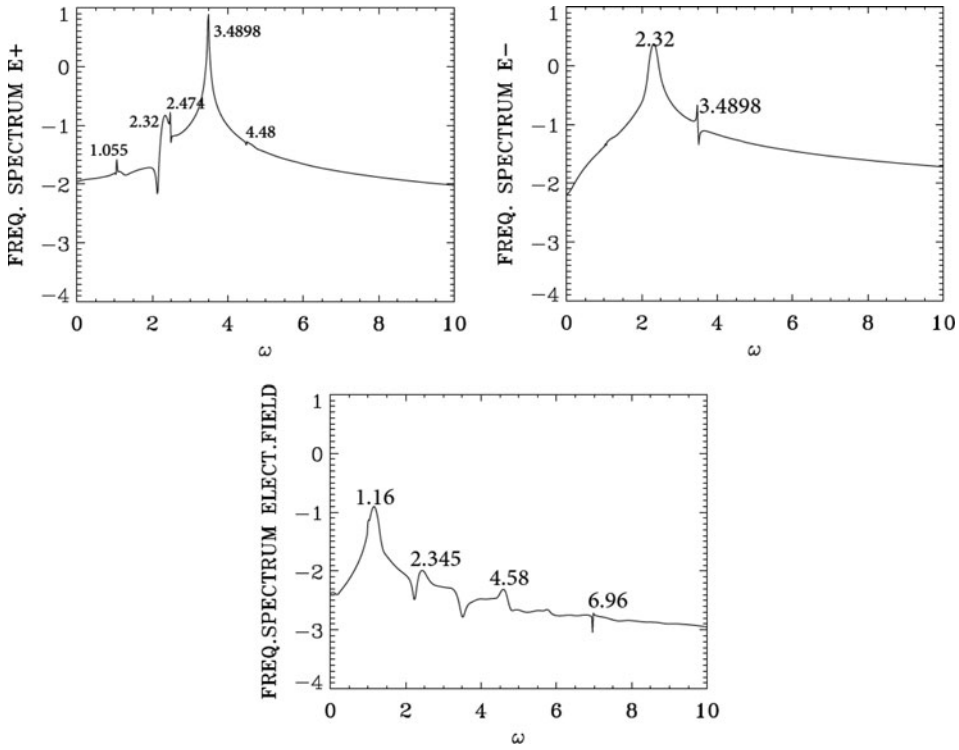

Fig. 19. Frequency spectra of (clockwise) the incident wave E^+, the backward wave E^-, and the longitudinal electric field E_x, at the position $x = 250$, at time $t = (623,951)$.

Figure 24 shows the growth of the vortices much more rapid than what is presented in Figure 13.

Figure 25 gives at $t = 1116$ the distribution function at $x = 60$ (left frame) and at $x = 100$ (right frame), spatially averaged over a wavelength. At $x = 60$, Figure 24 indicates we still are at in a transition showing growing vortices. At $x = 100$, the vortices seem to have reach a steady state. We look for the spatially averaged distribution function at $x = 100$. It shows a local minimum around $p_{xe} = 0.2$, around the phase of the saturated wave. By looking to the spectra of the system close to the left boundary at the end of the simulation in the domain $x = (20,184)$ in Figures 26 and 27 below, we get for the frequency of the longitudinal electric field the value 1.112 in Figure 27, and wavenumber of 5.484 in Figure 26, we deduce a phase velocity $\upsilon_{\text{phase}} \approx 0.20$, and a momentum $p_{\text{phase}} = \upsilon_{\text{phase}}/\sqrt{1-\upsilon_{\text{phase}}^2}$, from which $p_{\text{phase}} = 0.204$, very close to the local minimum we see in the plot of the distribution function on the right side of Figure 25.

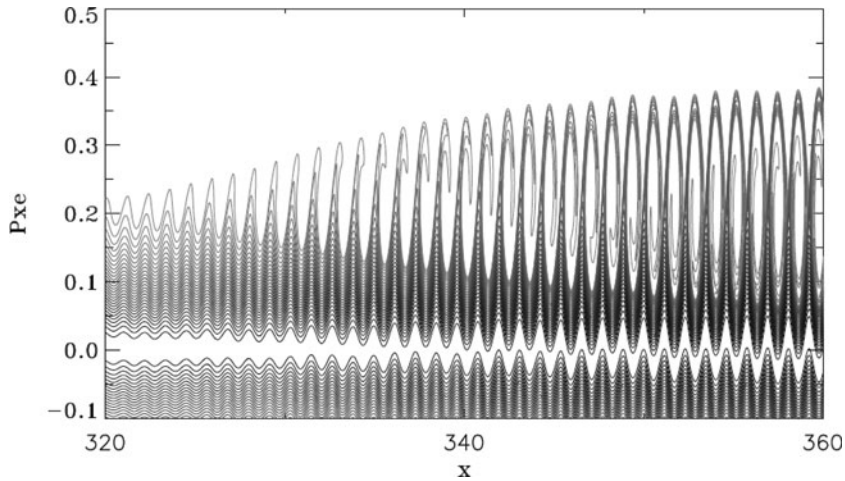

Fig. 20. Phase-space plot of the electron distribution function in the domain $x = (320,360)$, at time $t = 840$ at the arrival of the backward Raman scattered wave around $x = 320$.

https://doi.org/10.1017/S0263034616000495 Published online by Cambridge University Press

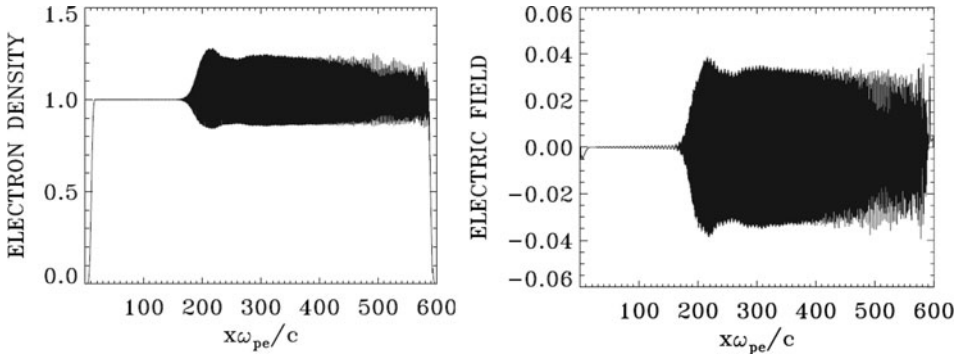

Fig. 21. Plot of the electron density profile (left frame) and the longitudinal electric field E_x (right frame) at time $t = 1000$.

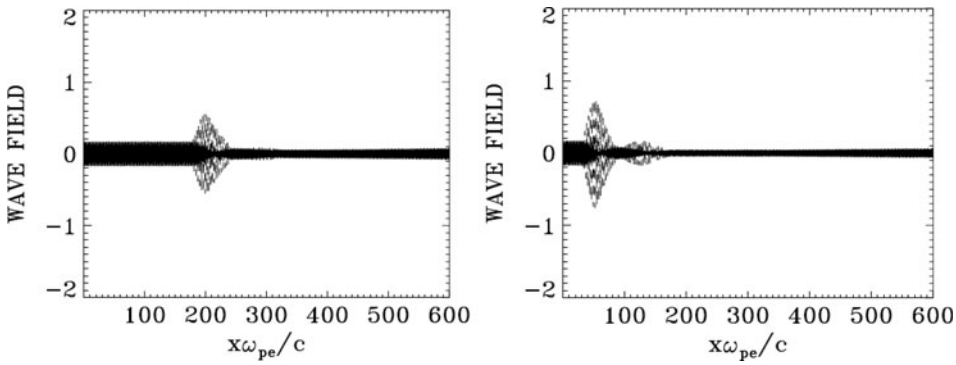

Fig. 22. The evolution of the incident forward pump wave E^+ (full curve), and the backward seed pulse E^- (dashed curve) at $t = 1000$ (left frame) and $t = 1116$ (right frame).

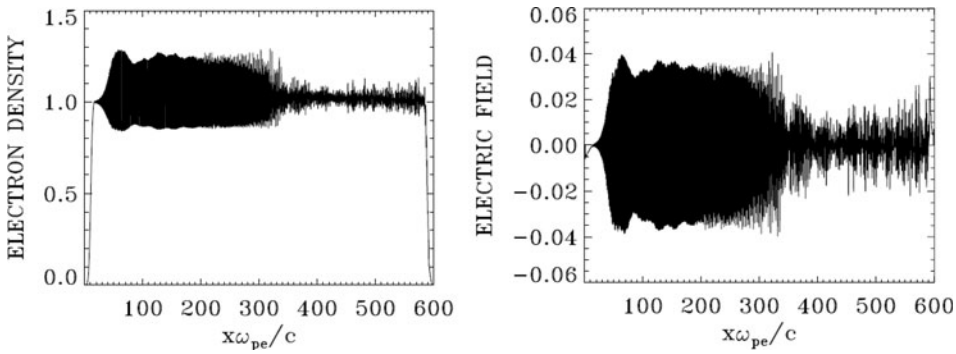

Fig. 23. Plot of the electron density profile (left frame) and the longitudinal electric field E_x (right frame) at time $t = 1116$.

Figure 26 presents the wavenumber spectra of the pump E^+, the backward wave E^-, and the longitudinal electric field. The frequency spectra in Figure 27 are obtained by taking the spectra of E^+, E^- and the longitudinal electric field, registered at $x = 250$ during the passage of the front of the pulse, from $t_1 = 920$ to $t_2 = 1084$. The spectrum of E^- has now the dominant modes, with a broad spectrum for the peak value. In Figure 26, the peak wavenumbers for E^- extend from 2.109 to 2.186. The peak at 2.186 is the same as the one we got in Figure 15, and the peak at 2.109 is close to the value of 2.063 calculated in Eq. (12) for the backscattered Raman wave. In Figure 27, the peak frequencies for E^- extend from 2.34 to 2.37. We also see the anti-Stokes at 4.52. The peak at 2.37 is the same as the one we see in Figure 16, and the peak at 2.34 is close to the frequency of 2.30 calculated in Eq. (11) for the frequency of the backscattered Raman wave. So in addition to the peaks we got in the study of the KEEN wave in Section 3.1, we have in the present case a clear coupling with the backscattered Raman wave. We are far from the picture of a single

https://doi.org/10.1017/S0263034616000495 Published online by Cambridge University Press

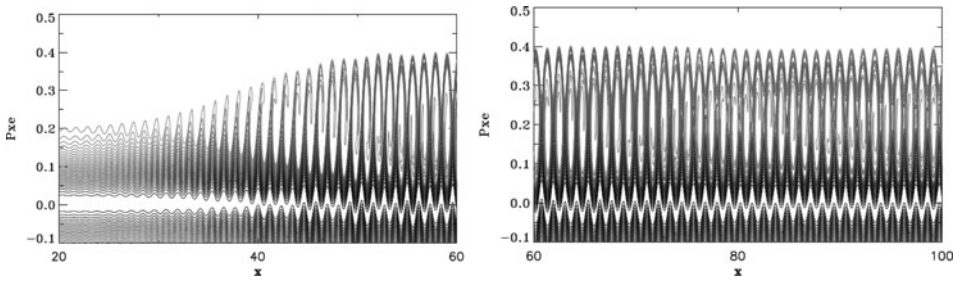

Fig. 24. Phase-space plot of the electron distribution function in the domain $x = (20,100)$, showing the vortices in the front edge at time $t = 1116$.

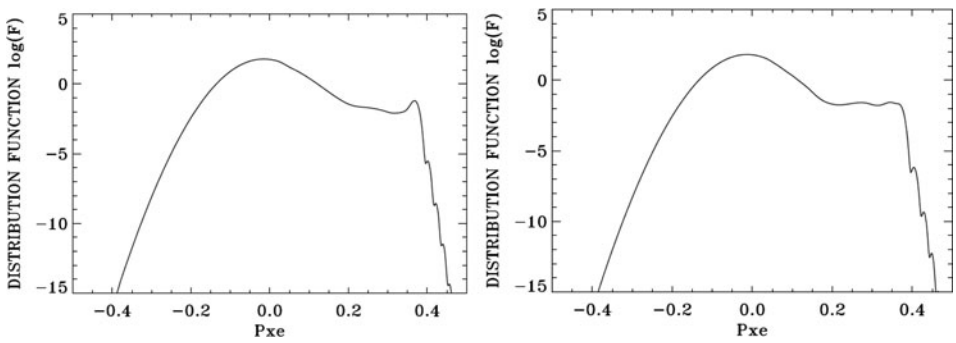

Fig. 25. The distribution function spatially averaged over a wavelength around the positions $x = 60$ (left frame), and $x = 100$ (right frame), at time $t = 1116$.

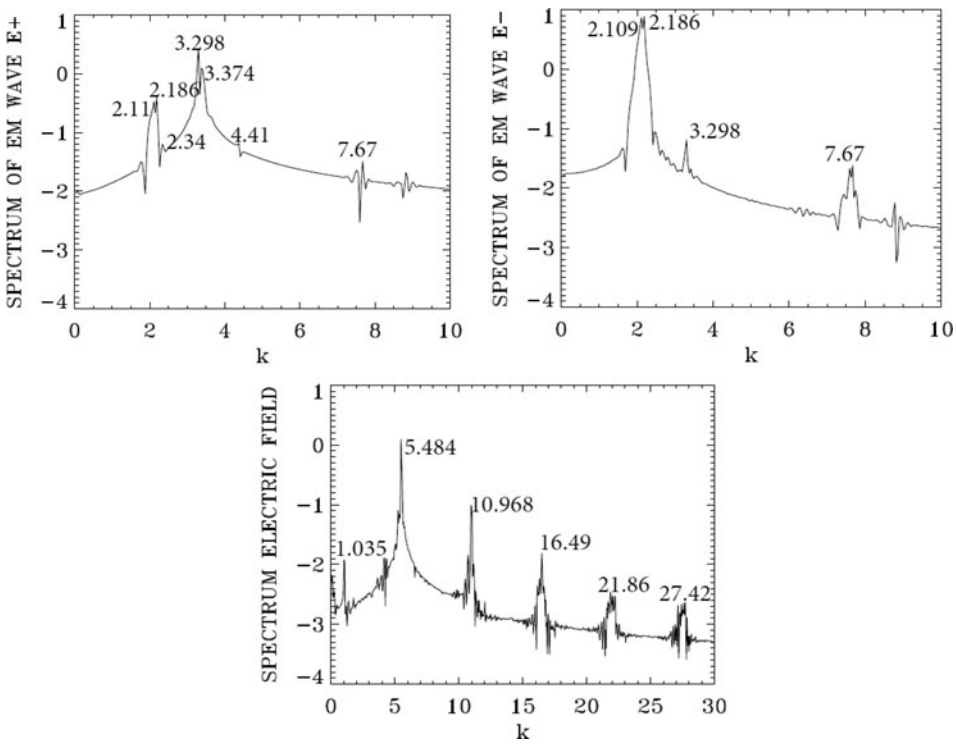

Fig. 26. Wavenumber spectra of (clockwise) the incident wave E^+, the backward wave E^-, and the longitudinal electric field E_x, in the domain $x = (20,184)$ at $t = 1116$.

https://doi.org/10.1017/S0263034616000495 Published online by Cambridge University Press

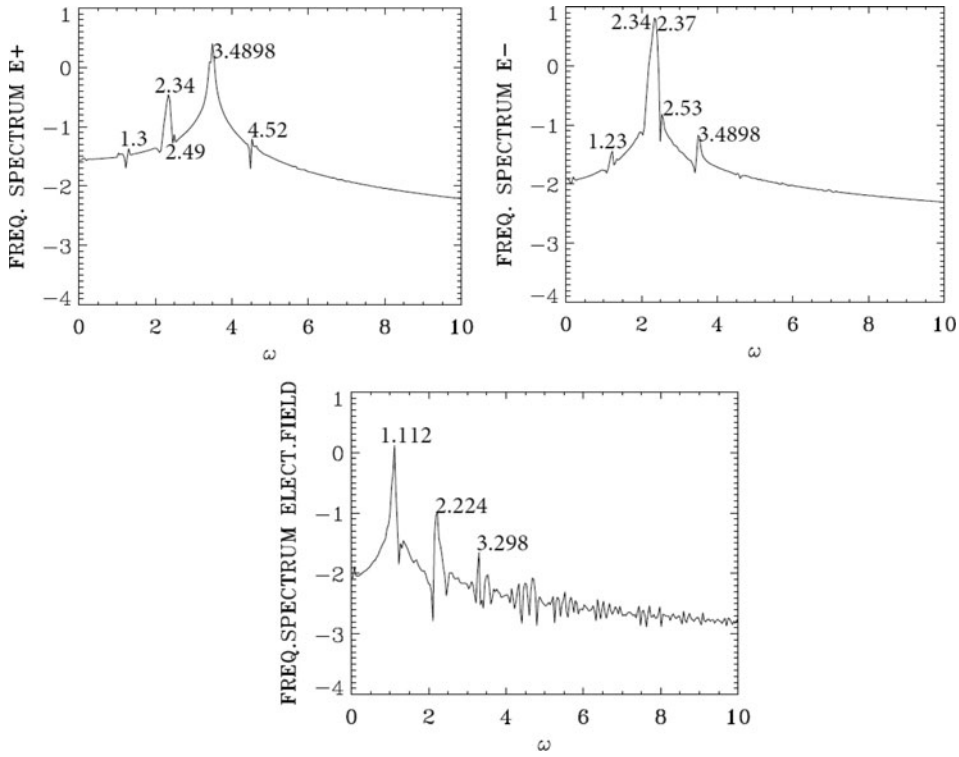

Fig. 27. Frequency spectra of (clockwise) the incident wave E^+, the backward wave E^-, and the longitudinal electric field E_x, at the position $x = 250$, at time $t = (920,1084)$.

peak mode dominating the final spectrum. The dominant E^- mode now dominates the mode coupling process. The wavenumbers of 2.109 and 2.186 are also appearing in the spectrum of E^+. The pump has shifted slightly to 3.298. We also see the anti-Stokes wavenumber at 4.41. We see in Figure 26, in the spectrum of the longitudinal electric field, the wavenumber coupling $3.298 \approx -2.186 + k_{eB}$ leads to $k_{eB} \approx 5.484$. We also see in Figure 26 the harmonics at 10.968, 16.59, 21.86, and 27.42. The peak in E^- at the wavenumber 2.186 would also interact with the peak at 5.485 of the longitudinal electric field to $-2.186 = -k + 5.484$, from which the mode at $k = 7.67$, which appears in the spectrum of E^- in Figure 26. It also appears in the forward direction in the spectrum of E^+ $7.67 = 2.186 + 5.484$. Also in the spectrum of E^+ the peak at 3.298 and the peak at 8.78 (not indicated in the figure) can couple $8.78 = 3.298 + 5.484$.

We see in Figure 27 in the frequency spectrum of E^- the dominant backward pulse dominated by the peaks at 2.34–2.37 [calculated at 2.30 in Eq. (11)]. This peak appears in the spectrum of E^+. We also see the anti-Stokes frequency at 4.52. The plasma wave associated with the forward scattered mode now appears at the frequency $3.4898 \approx 2.34 + \omega_{eF}$ (and also for the backward scattered mode and the KEEN wave), from which $\omega_{eF} \approx 1.15$, very close to the broad peak at 1.112 which appears in the frequency spectrum of longitudinal electric field (together with harmonics).

4. ANOTHER EXAMPLE OF SEED PULSE AMPLIFICATION

We now analyze the results of a simulation using parameters similar to those presented in Mourou *et al.* (2012). In the present calculation, $n/n_{cr} = 0.1$, which corresponds in this case to the pump wave frequency of the injected laser beam $\omega_{0P} = 1/\sqrt{n/n_{cr}} = 3.481$ (normalized to the plasma frequency ω_{pe}, n_{cr} is the critical density for the pump). For the linearly polarized wave $a_0^2 = I\lambda_0^2/\ 1.368 \times 10^{18}$, I is the laser intensity in W/cm^2, and λ_0 the laser wavelength in microns In the present calculation the wavelength of the pump is $\lambda_{0P} = 1.05$ μm, and the laser intensity is $I_{0P} = 2 \times 10^{15}$ W/cm^2, which corresponds to an amplitude of the vector potential of the pump $a_{0P} = 0.04$. The seed Raman backscattered pulse has a frequency $\omega_{0B} = 2.1657$ and a wavelength $\lambda_{0B} = 1.541$ μm. The laser intensity is $I_{0B} = 1 \times 10^{14}$ W/cm^2, which corresponds to an amplitude of the vector potential of the seed pulse is $a_{0B} = 0.01318$.

The frequency and wavenumber (ω_{0P}, k_{0P}) of the pump wave are related in normalized units by the relation $\omega_{0P}^2 = 1 + k_{0P}^2$, from which $k_{0P} = 3.0185$. For the stimulated Raman scattering, or the coupling of a pump light wave to a daughter scattered light wave and an EPW, the values of the electron plasma wavenumber k_{eB} associated with the stimulated Raman backscattered mode SRBS, and k_{eF} associated with the stimulated Raman forward scattered mode SRFS are roots of Eq. (9). For the present problem we also have hydrogen ions with

https://doi.org/10.1017/S0263034616000495 Published online by Cambridge University Press

$M_i/M_e = 1836$. We assume an electron temperature $T_e = 0.2$ keV. In Eq. (9), the parameter $\mu = m_e c^2/\kappa T_e = c^2/\upsilon_{te}^2 = 1/(0.04424\sqrt{T_e})^2 = 2555$. The resulting roots of Eq. (9) are $k_{eB}\lambda_{De} = 0.09774$ for the plasma mode associated with the SRBS, and $k_{eF}\lambda_{De} = 0.0214$ for the plasma mode associated with the SRFS. In our normalized units the Debye length $\lambda_{De} = \upsilon_{te}/c = 0.04424\sqrt{T_e}$ (T_e is in keV), so $\lambda_{De} = 0.0198$ for $T_e = 0.2$ keV. We finally get $k_{eB} = 0.09774/\lambda_{De} = 4.94$ for the SRBS plasma wave, and $k_{eF} = 0.0214/\lambda_{De} = 1.0816$ for the SRFS plasma wave. The corresponding frequencies for the SRBS plasma wave and the SRFS plasma wave are solutions of Eq. (10). We get for the SRBS wave $\omega_{eB} = 1.0134$, and for the SRFS plasma wave $\omega_{eF} = 1.000$. The selection rules give the following results for the forward scattered electromagnetic wave (ω_{0F}, k_{0F}) and the backward scattered electromagnetic wave (ω_{0B}, k_{0B}):

$$\begin{aligned}\omega_{0B} &= \omega_{0P} - \omega_{eB} = 3.18 - 1.0134 = 2.166;\\ \omega_{0F} &= \omega_{0P} - \omega_{eF} = 3.18 - 1.000 = 2.18,\end{aligned} \tag{14}$$

$$\begin{aligned}k_{0B} &= k_{eB} - k_{0P} = 4.94 - 3.0185 = 1.9215;\\ k_{0F} &= k_{0P} - k_{eF} = 3.0185 - 1.081 = 1.9375.\end{aligned} \tag{15}$$

Note the close values of (ω_{0F}, k_{0F}) with (ω_{0B}, k_{0B}). We verify that the results in Eqs. (14) and (15) obey the dispersion relation of the electromagnetic wave $1 + k_{0F}^2 = \omega_{0F}^2$, (from which we get $\omega_{0F} = 2.18$), and $1 + k_{0B}^2 = \omega_{0B}^2$ (from which we get $\omega_{0B} = 2.166$). These results are in very good agreement with the results in Eq. (14). We note also the possibility of the anti-Stokes resonance according to the selection rules $\omega_{as} = \omega_{0P} + \omega_{eF} = 3.18 + 1.00 = 4.18$, $k_{as} = k_{0P} + k_{eF} = 3.0185 + 1.081 = 4.099$. We calculate from the relation $1 + k_{as}^2 = \omega_{as}^2$ a value $\omega_{as} = 4.219$, close to the value of 4.18 calculated from the selection rule. As discussed in Section 3, KEEN waves have been identified in Shoucri and Afeyan (2014), which do not belong to the dispersion relations presented in Eqs. (9) and (10) and resulted from the backscattering of the pump with the backward stimulated wave at (ω_{0F}, $-k_{0F}$). This results in a coupling very close to the coupling of the backscattered Raman wave (ω_{0B}, $-k_{0B}$), since as we previously noted in Eqs. (14) and (15), these values are very close.

The ions were included in the calculation but did not play any role in the physics except establishing a small self-consistent sheath at the edges. We use a fine resolution grid in phase space, with $N = 30{,}000$ grid points in space, and 800 grid points in momentum space for the electrons (extrema of the electron momentum are $\pm$ 1.2). We use the same plasma profile as in Section 3, with the same total length of the system of $L = 600c/\omega_{pe}$. In our normalized units $\Delta x = \Delta t = 0.02$. We also have $\Delta x/\lambda_{De} \approx 1.01$.

The forward propagating linearly polarized wave is injected in the domain at the left boundary at $x = 0$ with $E^+ = 2E_{0P}\cos(\omega_{0P}t)$, $E_{0P} = \omega_{0P}a_{0P}$, with $a_{0P} = 0.04$. The pump precursor reaches the right boundary at $t = 600$ (since in our normalized units $x = t$). A seed pulse is injected at $x = L$ in the backward direction in the form $E^- = -2E_{0B}P_{0B}(t)\cos\omega_{0B}\tau$, where $\omega_{0B} = 2.166$ and $\tau = t - t_1$. The temporal shape factor of the seed pulse is $P_{0B}(t)$ similar to the expression in Section 3, with $\tau_s = 6.2$, $t_2 = 600$, $t_0 = 580$, $t_1 = 560$, $t_1 < t < t_2$. $E_{0B} = \omega_{0B}a_{0B}$ with $a_{0B} = 0.01318$. In this way, the seed Gaussian pulse starts penetrating the domain from the right boundary at $t = t_1 = 560$. When the pump precursor has reached the right boundary $x = L = 600$ at $t = 600$, the seed pulse has fully penetrated from the right boundary, and its peak has reached the point at $x = 580$ at the time $t = 600$.

For the parameters used in this simulation, the SRFS plasma mode with $k_{eF}\lambda_{De} = 0.0214$ is very weakly damped (Bers *et al.*, 2009). No seed or initial perturbation is added to stimulate the more damped SRBS mode with $k_{eB}\lambda_{De} = 0.09774$. We present in Figure 28 the evolution of the incident pump E^+ wave (full curve) and the backward seed pulse E^- (dashed curve) at: (a) $t = 820$, (b) $t = 920$, (c) $t = 1160$, (d) $t = 1220$. The growth and contraction of the seed pulse (dashed curves), propagating toward the left, is obvious, and also the detachment of the front of the growing seed pulse. The constant amplitude full curve at the left is for the constant amplitude incident pump. Once the seed is reaching the same amplitude as the pump, we enter the regime of pump depletion. The smaller peaks we see behind the front pulse of the growing seed are due to the fact that when the pump depletes, the seed pulse can lose energy again for the pump, which results in the oscillations in the tail of the seed we observe (i.e. the amplified seed beats with the plasma wave to regenerate the pump, which results in the depletion of the seed). Also, the exchange with the anti-Stokes resonance can play a similar role in this oscillation.

We present in Figure 29 a plot of the electron density at $t = 1160$ and 1220, corresponding to Figures 28c and 28d, and in Figure 30 the electron density in the region of the front edge in $x \in (15, 65)$ at $t = 1220$. We observe regular oscillations in the front edge in $x \in (15, 65)$. The wavelength associated with these regular oscillations is the wavelength of the growing seed pulse, which is $\lambda_{eB} = 2\pi/k_{eB} = 1.27$, which is also very close to the value of λ_{eF} as we have mentioned from the results of Eq. (15). We shall see below that this corresponds to coherent vortical structures in phase-space, while the part of the density plots in Figure 29, which shows a rather noisy density profile to the right, corresponds to a region in phase space where vortices were actively merging.

This is also shown in Figure 31, where we present in the phase-space the contour plots of the electron distribution function in $x \in (15, 65)$, and in $x \in (65, 115)$ at $t = 1220$. In $x \in (15, 65)$, we observe a more coherent vortices structure (corresponding to the profile we see in Fig. 30), while in $x \in (65, 115)$ we see the vortices at the right of the figure who are coalescing together, leading to the somewhat noisy structure we see at the right the density plots in Figure 29.

https://doi.org/10.1017/S0263034616000495 Published online by Cambridge University Press

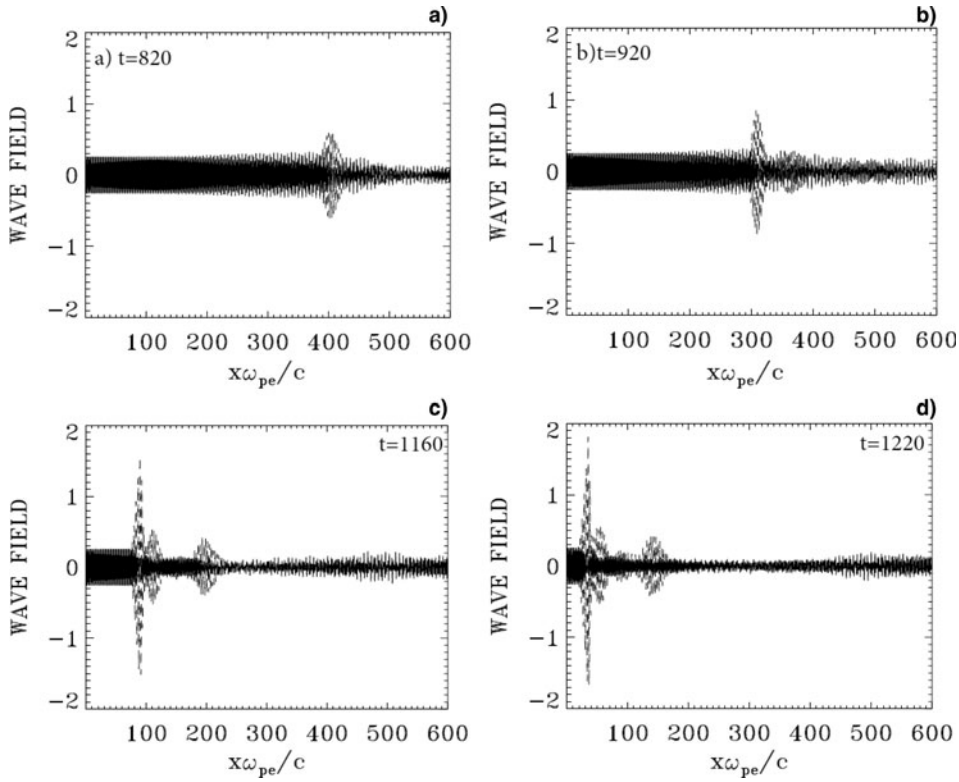

Fig. 28. Evolution of the incident pump E^+ wave (full curve) and the backward seed pulse E^- (dashed curve) at: (a) $t = 820$, (b) $t = 920$, (c) $t = 1160$, (d) $t = 1220$; $\tau_s = 6.2$ and $a_{0P} = 0.04$.

We present in Figure 32 the wavenumber spectra of the incident wave E^+, the backward wave E^- and the longitudinal electric field in the domain $x \in (140, 468)$ at the time $t = 640$, well before the backward injected seed reaches this part of the domain. The only excited waves in this case are due to the forward propagating pump E^+. We recognize the peak of the pump E^+ at $k_{0P} = 3.01$ [calculated at 3.0184 in our theoretical calculations in Eq. (15)]. The pump is exciting a weakly damped, forward propagating wave with wavenumber $k_{0F} = 1.936$, in agreement with our theoretical results in Eq. (15). We have also a very small peak for the anti-Stokes wavenumber at $k_{as} = 4.1034$ (calculated at 4.099 in our theoretical calculations). Since the plasma is a nonlinear medium, the same modes are appearing in the spectrum of the backward wave E^- at much lower amplitude, as previously explained. The wavenumber spectrum of the excited longitudinal electric field show the wavenumber of the resonant plasma mode for the forward wave at $k_{eF} = 1.0738$ (calculated at 1.081 in our theoretical calculations). The values of k_{0B} and k_{0F} in Eq. (15) are very close. The pump at 3.0104 in the spectrum of E^+ in Figure 32 can couple with the mode at 1.9366 in the spectrum of E^- to produce the plasma mode at $3.0104 = -1.9366 + k_{keen}$, or $k_{keen} = 4.977$, very close to the

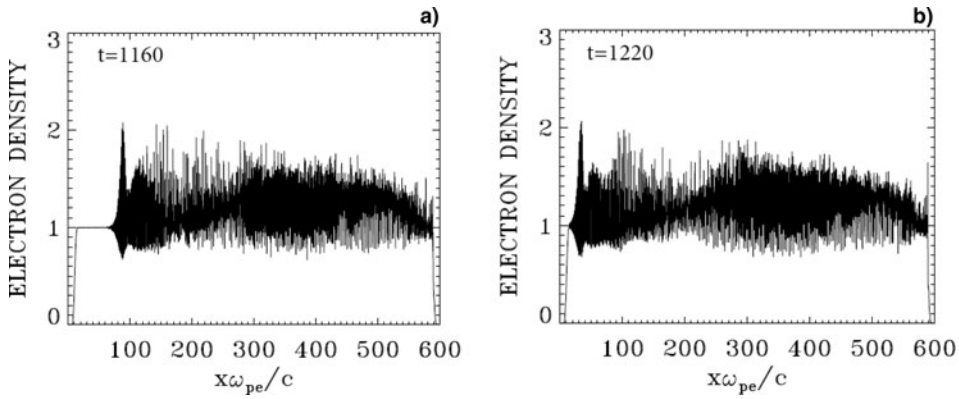

Fig. 29. Plot of the electron density profile at $t = 1160$ and 1220; $\tau_s = 6.2$ and $a_{0P} = 0.04$

https://doi.org/10.1017/S0263034616000495 Published online by Cambridge University Press

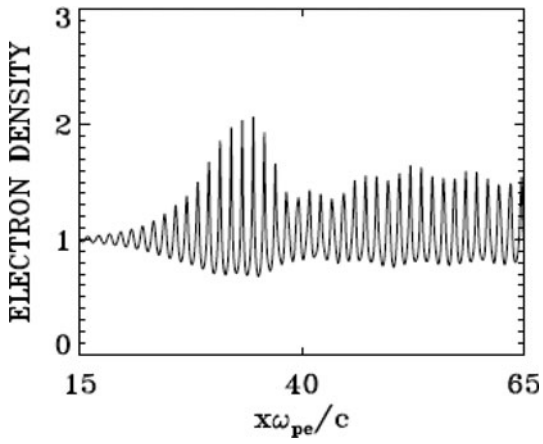

Fig. 30. Plot of the electron density in the region of the front edge in $x \in (15, 65)$ at $t = 1220$.

calculated plasma wave $k_{eB} = 4.94$ associated with the back-scattered Raman wave (the spectrum of the longitudinal electric field shows a peak at 4.966 in Fig. 32). So even though the seed pulse is still far away, there is a small plasma mode at 4.966 excited well before the arrival of the seed pulse, associated with the backward resonance due to the coupling of the pump at $k_{0P} = 3.0104$ in E^+ (which is exciting the forward scattered mode at $k_{0F} = 1.936$), with the backward mode appearing at 1.936 in the spectrum of E^- in Figure 31. So the pump is exciting the plasma mode around 4.96 through two backward resonances. A backward resonance with the KEEN wave $3.0104 = -1.936 + 4.977$, and the resonance with the seed pulse, which still did not take place in the spectra in Figure 32 at $t = 600$. Finally for the linearly polarized wave, we have a plasma mode appearing in the spectrum of the longitudinal wave at the harmonic of the pump $2k_{0p} = 6.04$ (calculated at 6.036 in our theoretical results), as explained in Eq. (13). The forced oscillations at the wavenumber 6.04 further stimulate the mode at 4.966, by coupling with the plasma wave at 1.0738, through the selection rule $6.04 = 4.966. + 1.0738$. Also a longitudinal mode appears at 7.1138 through the coupling $7.1138 = 6.040 + 1.0738$.

Figure 33 presents the frequency spectra of the pump wave E^+, the backward wave E^- and the longitudinal electric field, from the data recorded at the position $x = 150$ between $t_1 = 492$ and $t_2 = 819$, before the arrival of the backward propagating pulse. The spectrum of E^+ in Figure 33 shows the pump frequency at 3.183 [calculated 3.18 in Eq. (14)], the forward scattered mode at 2.183 [calculated at 2.18 in Eq. (14)]. The anti-Stokes mode is at 4.18 (calculated at 4.18). These same modes appear in the spectrum of E^- in Figure 33 as previously explained. We see a mode of frequency 1.00 in the frequency spectrum of the longitudinal electric field excited though the forward coupling $3.183 = 2.183 + 1.00$. We also see the mode at the harmonic of the pump $2\omega_{0p} = 6.366$ as explained in Eq. (13). And the coupling of the pump with the wave at $(\omega_{0F}, -k_{0F})$ produces a KEEN wave as explained in Section 3, with frequency $3.183 = 2.183 + \omega_{keen}$, from which $\omega_{keen} = 1.00$. Note the mode at 5.369 which can be excited through the forced oscillation $1.00 + 5.369 = 6.369$, very close to the forced oscillation at 6.366. We also note in Figure 33 the possible further forced resonance $3.183 + 2.183 = 5.366$, very close to the mode at 5.369.

We look again in Figure 34 to the wavenumber spectra in the same domain $x \in (140, 468)$, the same domain as in Figure 32, but at the time $t = 740$, when the backward pulse has entered the domain $x \in (140, 468)$. The spectrum of E^+ is essentially the same as in Figure 32, however the mode at 1.936 is more stimulated. The spectrum of E^- in Figure 34 however shows the effect of the arrival of the pulse. There is a broad peak. We are still in a transient phase, and this broad peak is due to the presence of the mode at 1.936 which results from the forward coupling of the pump $3.010 = 1.936 + 1.074$ (the mode in the spectrum of the longitudinal electric field appears at 1.073), the KEEN wave coupling $3.010 = -1.936 + k_{keen}$, from which $k_{keen} = 4.946$, which we see in the spectrum of the longitudinal electric field. Finally, the frequency of the arriving pulse from Eq. (14) is at $\omega_{0B} = 2.166$, and should result in a wavenumber response in E^- at $k_{0B} = 1.921$ (precisely in the broad peak we observe in the spectrum of E^- in Fig. 34), and in

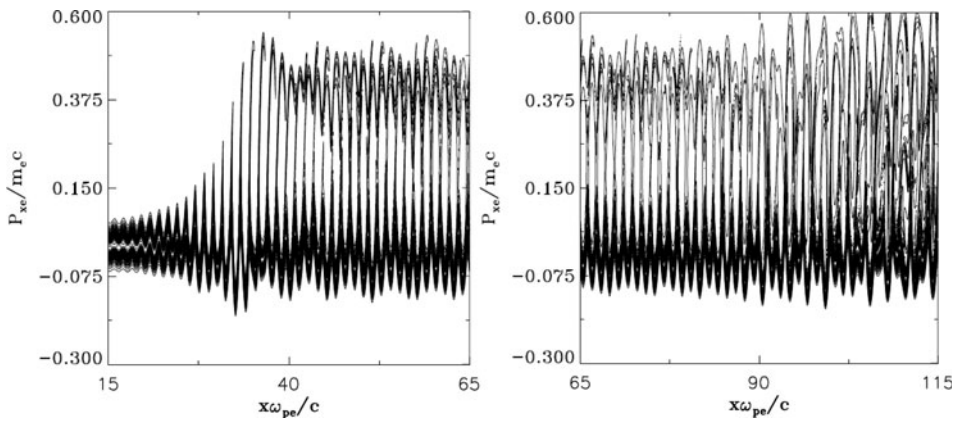

Fig. 31. Phase-space plot of the electron distribution function in $x \in (15, 65)$ and in $x \in (65, 115)$, at $t = 1220$.

https://doi.org/10.1017/S0263034616000495 Published online by Cambridge University Press

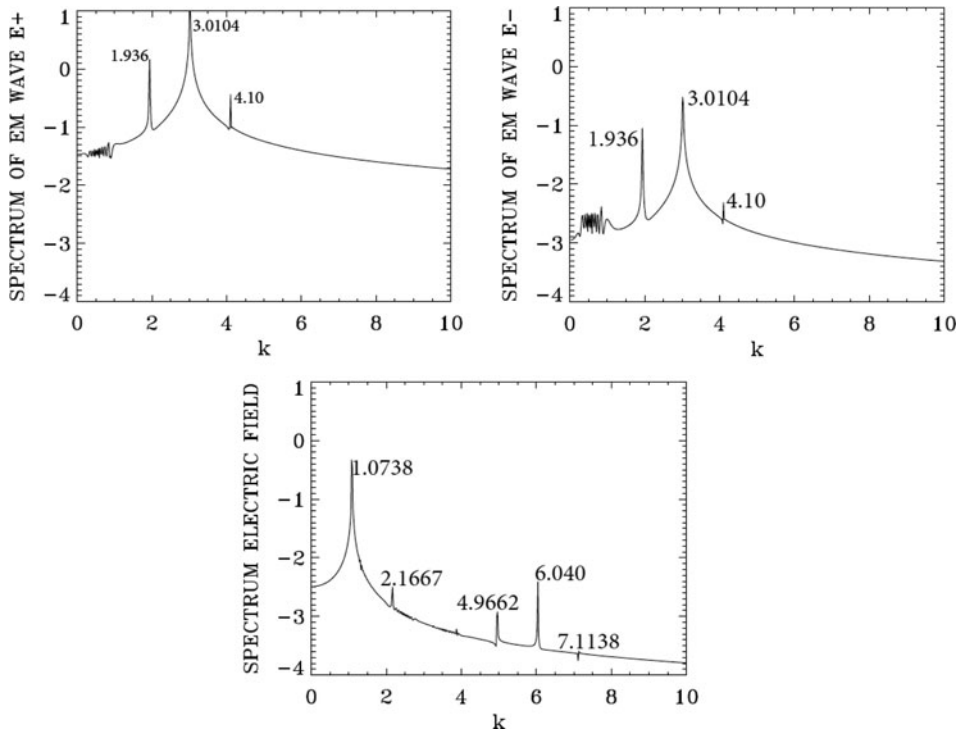

Fig. 32. Wavenumber spectra of (clockwise) the incident wave E^+, the backward wave E^- and the longitudinal electric field in the domain $x \in (140, 468)$ at time $t = 640$.

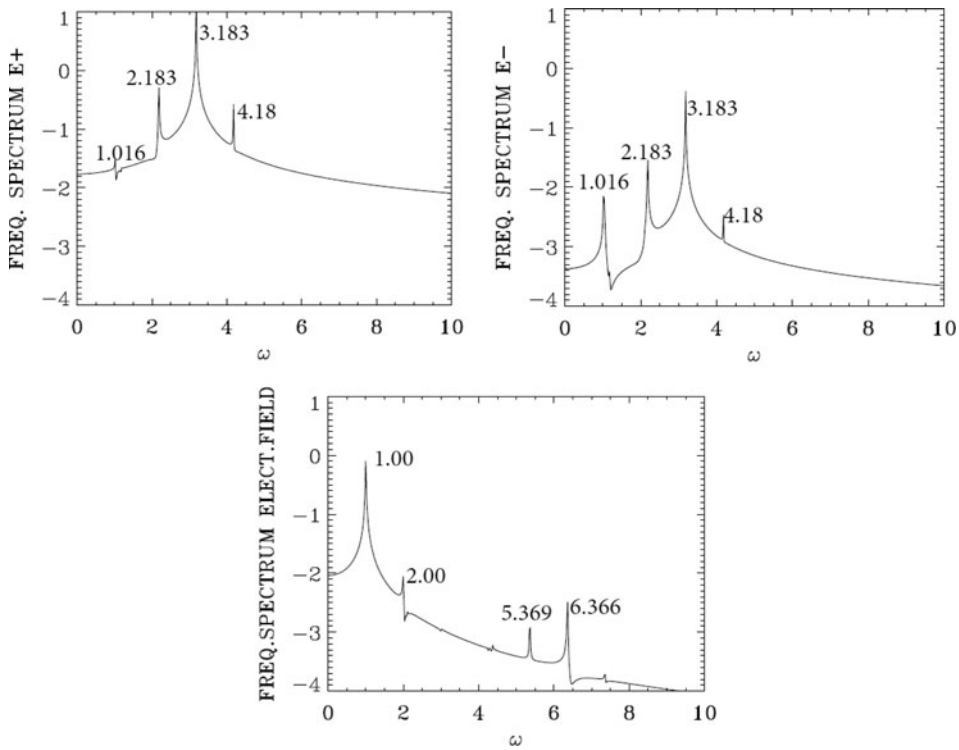

Fig. 33. Frequency spectra of (clockwise) the incident wave E^+, the backward wave E^-, and the longitudinal electric field E_x, at the position $x = 150$, at time $t = (192,819)$.

https://doi.org/10.1017/S0263034616000495 Published online by Cambridge University Press

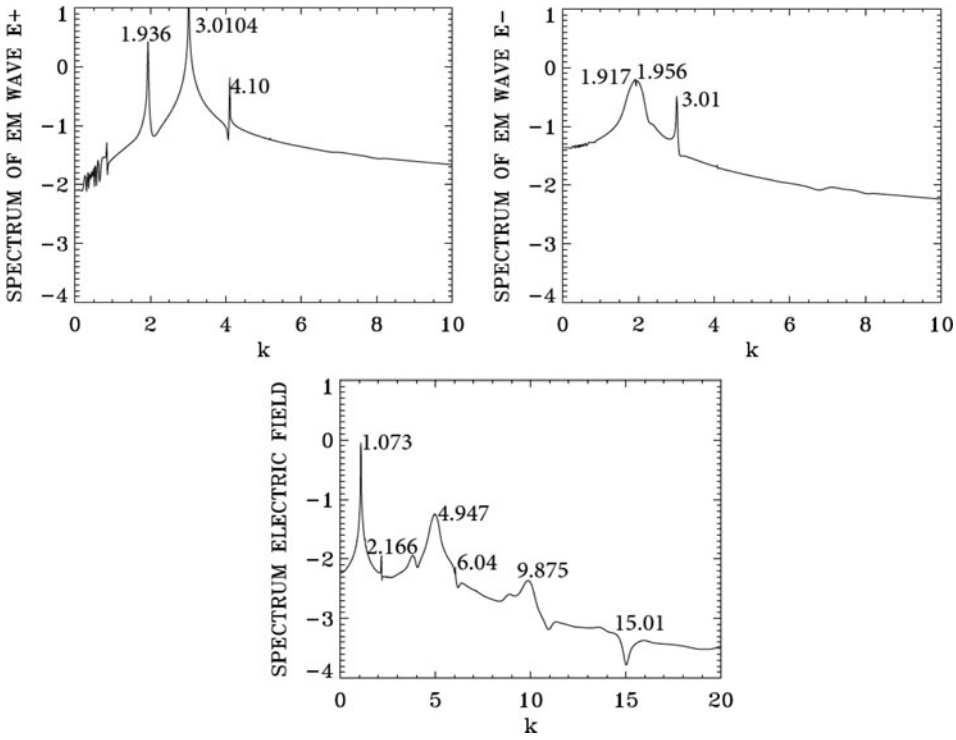

Fig. 34. Wavenumber spectra of (clockwise) the incident wave E^+, the backward wave E^- and the longitudinal electric field in the domain $x \in (140, 468)$ at time $t = 740$.

a wavenumber of the longitudinal electric field at $k_{eB} = 4.94$ (see the broad peak in Fig. 34). So the peak at 4.947 results from the excitation of the KEEN wave $k_{keen} = 4.946$ and of the plasma wave to the SRBS at $k_{eB} = 4.94$. See also the growing harmonics of the mode at 4.947, in the spectrum of the longitudinal electric field in Figure 34.

Figure 35 presents the wavenumber spectra at the end of the simulation at $t = 1220$, in the domain $x \in (30, 194)$. The peak of the pump is now at 3.03 in the spectrum of E^+, also appearing in a broad spectrum around 3.1 in the spectrum of E^- in Figure 35. The dominant mode is now in the spectrum of the amplified seed in E^-, where we see in Figure 35 a broad spectrum between 1.917 and 2.147 (these are peaks of the backward seed wave initially calculated at 1.921, and the peak at 1.937 identified as a backscattered KEEN wave as discussed for the spectrum of E^- in Fig. 34). These two peaks are appearing also in the spectrum of E^+ in Figure 35. These are also analogous to the broad double peaks we observe in the spectrum of E^- in Figure 26, due to the backscattered Raman wave and the backscattered KEEN wave. The anti-Stokes at $k_{as} \approx 4.1$ is also present in E^+ and E^-. The spectrum of the longitudinal electric field in Figure 35 shows the peak of the plasma wave associated with the forward Raman scattering at $k_{eF} = 1.073$ [calculated at 1.081 in our theoretical results from Eq. (14)]. Also the plasma wave associated with the backward Raman scattering at $k_{eB} = 5.023$ [calculated at 4.94 in our theoretical results in Eq. (15)], and the scattering of the pump with the mode at 2.147 in the spectrum of E^-, which results in a KEEN wave as previously explained in the results presented in Figure 35.

The frequency spectra we present in Figure 36 are calculated by monitoring the fields at the position $x = 150$, for the values of time $t \in (1050, 1214)$. The theoretical value of the pump frequency at $\omega_{0P} = 3.18$ is appearing in the frequency spectrum of E^+ in a broad peak around 3.144. The frequency spectrum is now dominated by the backward seed wave, we see a broad peak around 2.147 and 2.3 in the frequency spectrum of E^- [theoretical values calculated in Eq. (14) are for the backscattered Raman wave at 2.166 and for the backscattered KEEN wave 2.18]. These peaks are also present in frequency spectrum of E^+ around the peaks at 2.186 and 2.3. The dominant E^- wave is now interacting with the pump and shifting frequency at 3.22 in the frequency spectrum of E^-. The anti-Stokes frequency calculated at 4.18 is indeed at 4.18 in the frequency spectrum of E^+, and appears also around 4.29 in the frequency spectrum of E^-. The frequency spectrum of the longitudinal electric field shows a broad peak at $\omega_{eB} = 1.00$. The frequency of the plasma wave associated with the backward Raman scattering is calculated at 1.0134 in our theoretical results. The theoretical value of the frequency of the plasma wave associated with forward Raman scattering is $\omega_{eF} = 1.00$. We have in Figure 36 for the longitudinal plasma wave a broad frequency around 1.00, extending to lower values with respect to the plasma frequency, which would denote a variation of the nature of the plasma wave to that of a KEEN wave (Afeyan *et al.*, 2004, 2014; Mehrenberger *et al.*, 2013;

https://doi.org/10.1017/S0263034616000495 Published online by Cambridge University Press

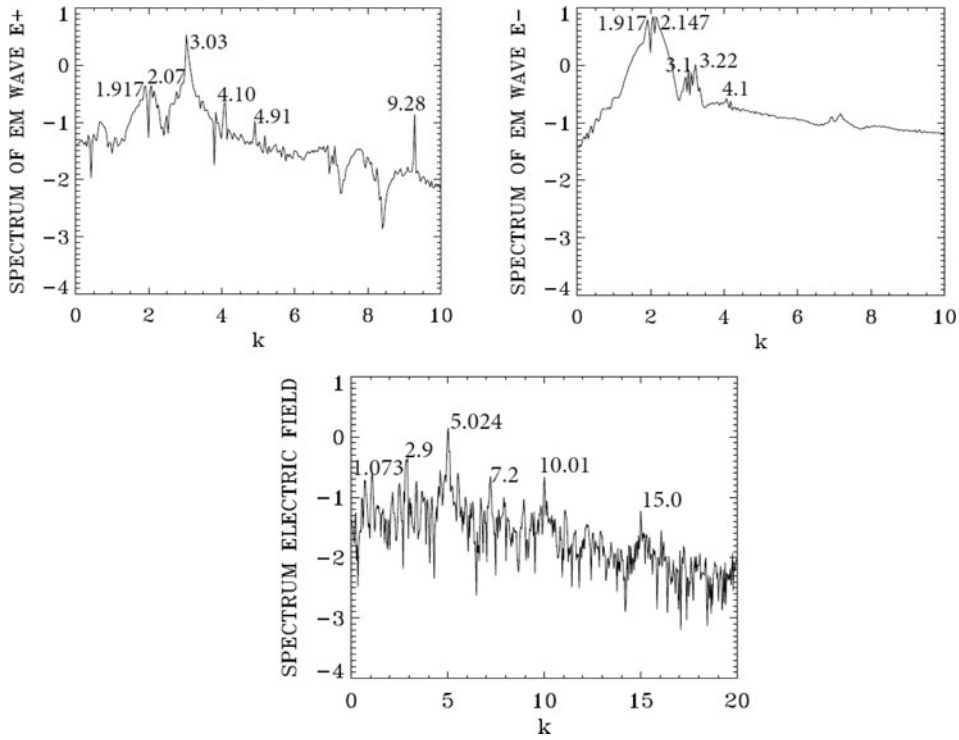

Fig. 35. Wavenumber spectra of (clockwise) the incident wave E^+, the backward wave E^- and the longitudinal electric field in the domain $x \in (30, 194)$ at time $t = 1220$.

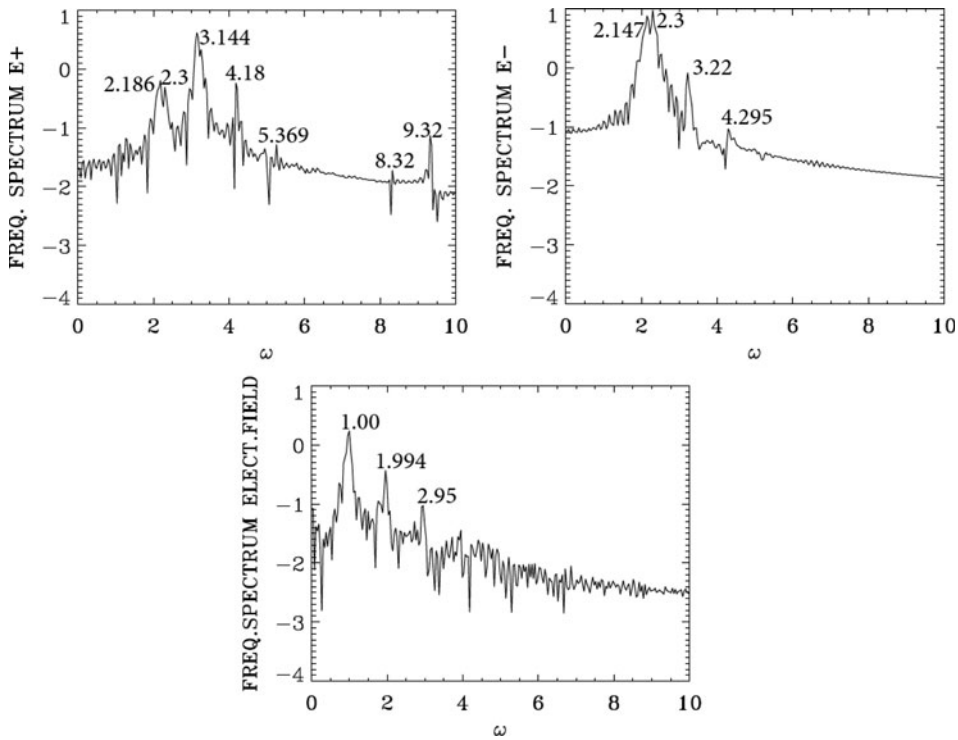

Fig. 36. Frequency spectra at the position $x = 150$ for the time $t = (1050, 1214)$, for (clockwise) the forward wave E^+, the backward wave E^-, and the longitudinal electric field.

https://doi.org/10.1017/S0263034616000495 Published online by Cambridge University Press

Shoucri & Afeyan, 2014). Note the multiple harmonics structures in the plasma wave.

5. CONCLUSION

The amplification of ultra-short seed pulses by SRB has been investigated using a relativistic Vlasov–Maxwell code in one spatial and one velocity dimension, which allows the inclusion of kinetic (non-collisional) effects in the modeling. We have identified the excitation of KEEN waves (Afeyan *et al.*, 2004, 2014; Mehrenberger *et al.*, 2013; Shoucri & Afeyan, 2014) and their participation in the SRBS process, when self-consistently modified distribution functions arise during the evolution of the system. In Shoucri and Afeyan (2014), KEEN waves were shown to result from the beating of the pump wave with the mode at $(\omega_{0F}, -k_{0F})$, where the mode (ω_{0F}, k_{0F}) is the SRFS mode. Here too, we see that phenomenon occur. The interesting physics demonstrated here is how SKEENS coexisting with SRBS *segregate* into a double vortex structure where SKEENS enhances SRBS amplification and where vortex merging causes more turbulent final states which are far less hospitable to clean, three mode amplification.

The fundamental question is whether SKEENS can be relied upon to amplify pulses *instead* of SRBS or whether it is their combined two-step action that is most beneficial. In addition, the long standing assertion that pi pulses, which are self-similar solutions, are viable when beams are finite in transverse extent and with intensity fluctuations (speckle patterns) that can be as large as 10:1 in intensity inside and out of speckles. Such intensity variations will not allow spatially uniform pump depletion based pulse compression, or amplification-halting to occur uniformly inside the beam volume. That means the beam will not be of one temporal width but be made up of components of different pulse shapes, as one traverses in and out of laser speckles. Such pulses will not have the desirable properties of being uniformly amplified and compressed at the same time. Other kinetic effects due to phase space vortices and their merger further complicate the pulse amplification and compression reliability of SRBS. This is seldom acknowledged in the pi pulse invoking literature. We caution against this expectation and point out that no experimental attempt to achieve such pulses has succeeded in plasmas to date. A new avenue of investigation is to generate and exploit KEEN waves and SKEENS as a means of nonlinearly transferring energy from a pump to a series of scattered waves with correlated features as described in this paper.

ACKNOWLEDGEMENTS

M. Shoucri is grateful to Dr. Réjean Girard for his constant support, and to the Centre de Calcul Scientifique de l'IREQ (CASIR) for the computer time used in the simulations presented in the present work. The work of BA was sponsored by a grant from AFSOR:FA955015C0036.

REFERENCES

Afeyan, B., Casas, F., Crouseilles, N., Dodhy, A., Faou, E., Mehrenberger, M. & Sonnendrucker, E. (2014). Simulations of kinetic electrostatic electron nonlinear (KEEN) waves with variable velocity resolution grids and high-order time-splitting. *Eur. Phys. J. D* **68**, 295/1–21.

Afeyan, B., Chou, A.E., Matte, J.P., Town, R.P.J. & Kruer, W.J. (1998). Kinetic theory of electron-plasma and ion acoustic waves in nonuniformly heated laser plasmas. *Phys. Rev. Lett.* **80**, 2322.

Afeyan, B., Won, K., Savchenko, V., Johnston, T., Ghizzo, A. & Bertrand, P. (2004). Kinetic electrostatic electron nonlinear (KEEN) waves and their interactions driven by the ponderomotive force of crossing laser beams. In *Proc. Int. Fusion Sciences and Applications* (Hammel, B., Meyerhofer, D., Meyer-ter-Vehn, J. and Azechi, H., Eds.), p. 213. La Grange Park, IL: American Nuclear Society. See arXiv:1210.8105.

Benisti, D., Yampolsky, N.A. & Fisch, N.J. (2012). Comparison between nonlinear kinetic modelings of stimulated Raman scattering using envelope equations. *Phys. Plasmas* **19**, 013110.

Bers, A., Shkarofsky, I. & Shoucri, M. (2009). Relativistic Landau damping of electron plasma waves in stimulated Raman scattering. *Phys. Plasmas* **16**, 022104/1–6.

Drake, J.F., Kaw, P.K., Lee, Y.C., Schmidt, G., Liu, C.S. & Rosenbluth, M.N. (1974). Parametric instabilities of electromagnetic waves in plasmas. *Phys. Fluids* **17**, 778.

Fisch, N.J. & Malkin, M.V. (2003). Generation of ultrahigh intensity laser pulses. *Phys. Plasmas* **10**, 2056.

Forslund, D.W., Kindel, J.M. & Lindman, E.L. (1975). Theory of stimulated scattering processes in laser-irradiated plasmas. *Phys. Fluids* **18**, 1002.

Ghizzo, A., Bertrand, P., Shoucri, M., Feix, M., Johnston, T.W., Fijalkow, E. & Feix, M. (1990). A vlasov code for the numerical solution of stimulated Raman scattering. *J. Comput. Phys.* **90**, 431–457.

Kruer, W. (1988) *The Physics of Laser-Plasma Interaction*. Boulder, CO: Addison-Wesley.

Lancia, L., Marquès, J.R., Nakatsutsumi, M., Riconda, C., Weber, S., Hüller, S., Mancic, A., Antici, P., Tikhonchuk, V.T., Heron, A., Audebert, P. & Fuchs, J. (2010). Experimental evidence of short light amplification using strong-coupling stimulated Brillouin scattering in the pump depletion regime. *Phys. Rev. Lett.* **104**, 025001/1–4.

Lehmann, G., Schluck, F. & Spatschek, K.H. (2012). Regions of Brillouin seed pulse growth in relativistic laser–plasma interaction. *Phys. Plasmas* **19**, 093120.

Lehmann, G. & Spatschek, K.H. (2013). Nonlinear Brillouin amplification of finite-duration seeds in the strong coupling regimes. *Phys. Plasmas* **20**, 073112/1–10.

Lehmann, G. & Spatschek, K.H. (2014). Non-filamental ultra-intense and ultra-short pulse fronts in three-dimensional Raman seed amplification. *Phys. Plasmas* **21**, 053101/1–14.

Lehmann, G., Spatschek, K.H. & Sewell, G. (2013). Pulse shaping during Raman-seed amplification for short laser pulses. *Phys. Rev. E* **87**, 063107/1–9.

https://doi.org/10.1017/S0263034616000495 Published online by Cambridge University Press

Malkin, V.M. & Fisch, N.J. (2005). Manipulating ultra-intense laser pulses in plasmas. *Phys. Plasmas* **12**, 044507.

Malkin, V.M., Shvets, G. & Fisch, N.J. (1999). Fast compression of laser beams to highly overcritical powers. *Phys. Rev. Lett.* **82**, 4448–4451.

Malkin, V.M., Toroker, Z. & Fisch, N.J. (2014). Saturation of the leading spike growth in the backward Raman amplifiers. *Phys. Plasmas* **21**, 093112/1–5.

Max, C.E., Arons, J. & Langdon, A.B. (1974). Self-modulation and sel-focusing of electromagnetic waves in plasmas. *Phys. Rev. Lett*. **33**, 209–212.

Mehrenberger, M., Steiner, C., Maaradi, L., Crouseilles, N., Sonnendrücker, E. & Afeyan, B. (2013). Vlasov on GPU (VOG Project). *ESAIM Proc*. **43**, 37.

Mourou, G.A., Fisch, N., Malkin, V., Toroker, Z., Khazanov, E., Sergeev, A., Tajima, T. & LeGarrec, B. (2012). Exawatt–Zetawatt pulse generation and applications. *Opt. Commun*. **285**, 720.

Ren, J., Cheng, W., Li, S. & Suckewer, S. (2007). A new method for generating ultraintense and ultrashort laser pulses. *Nat. Phys*. **3**, 732–736.

Riconda, C., Weber, S., Lancia, L., Marquès, J-R., Mourou, G.A. & Fuchs, J. (2013). Spectral characteristics of ultra-short laser pulses in plasma amplifiers. *Phys. Plasmas* **20**, 083115.

Shoucri, M. (2008*a*). Numerical simulation of wake-field acceleration using an Eulerian Vlasov code. *Commun. Comput. Phys*. **4**, 703–718.

Shoucri, M. (2008*b*). *Numerical Solution of Hyperbolic Differential Equations*. New York: Nova Science Publishers, Inc.

Shoucri, M. & Afeyan, B. (2014). Numerical simulation of Raman Scattering with a relativistic Vlasov–Maxwell code: A cascade of nonstationary nonlinear kinetic interactions. In *Computational and Numerical Simulations* (Awrejcewicz, J., Ed.), pp. 251–282. Croatia: InTECH Publ.

Shoucri, M., Gerhauser, H. & Finken, K.H. (2003). Integration of the Vlasov equation along characteristics in one and two dimensions. *Comput. Phys. Commun*. **154**, 65–75.

Shoucri, M., Matte, J.P. & Vidal, F. (2015). Relativistic Eulerian Vlasov simulations of the amplification of seed pulses by Brillouin backscattering in plasmas. *Phys. Plasmas* **22**, 053191.

Sircombe, N.J., Arber, T.D. & Dendy, R.O. (2006). Aspects of electron acoustic wave physics in laser backscatter from plasmas. *Plasma Phys. Control. Fusion* **48**, 1141–1153.

Spatschek, K.H. (1976). Parametrische instabilitäten in plasmen. *Fortschr. Phys*. **24**, 687–729.

Strozzi, D.J., Williams, E.A., Langdon, A.B. & Bers, A. (2007). Kinetic enhancement of Raman backscatter, and electron acoustic Thomson scatter. *Phys. Plasmas* **14**, 013104/1–13.

Strozzi, D.J., Williams, E.A., Langdon, A.B., Bers, A. & Brunner, S. (2010). Eulerian–Lagrangian kinetic simulations of laser–plasma interactions. In *Eulerian Codes for the Numerical Solution of the Kinetic Equations of Plasmas* (Shoucri, M., Ed.), pp. 89–122. New York: Nova Science Publishers, ISBN 978 1 61668 413 6.

Toroker, Z., Malkin, V.M. & Fisch, N. (2014). Backward Raman amplification in the Langmuir wavebreaking regime. *Phys. Plasmas* **21**, 113110/1–10.

Trines, R.M.G.M., Fiuza, F., Bingham, R., Fonseca, R.A., Silva, L.O., Cairns, R.A. & Norreys, P.A. (2011*a*). Production of picosecond, kilojoule, and petawatt laser pulses via Raman amplification of nanosecond pulses. *Phys. Rev. Lett*. **107**, 105002.

Trines, R.M.G.M., Fiuza, F., Bingham, R., Fonseca, R.A., Silva, L.O., Cairns, R.A. & Norreys, P.A. (2011*b*). Simulations of efficient Raman amplification into the multipetawatt regime. *Nat. Phys*. **7**, 87–92.

Valentini, F., O'Neil, T.M. & Dubin, D.H.E. (2006). Excitation of nonlinear electron acoustic waves. *Phys. Plasmas* **13**, 052303/1–7.

Vu, H.X., DuBois, D.F. & Bezzerides, B. (2007). Inflation threshold: A nonlinear trapping-induxed threshold for the rapid onset of stimulated Raman scattering form a single laser speckle. *Phys. Plasmas* **14**, 012702.

Wang, T.-L., Clark, D.S., Strozzi, D.J., Wilks, S.C., Martins, S.F. & Kirkwood, R.K. (2010). Particle-in-cell simulations of kinetic effects in plasma based backward Raman amplification in underdense plasmas. *Phys. Plasmas* **17**, 023109/1–9.

Yin, L., Daughton, W., Albright, B.J., Bowers, K.J., Montgomery, D.S., Kline, J.L., Fernandez, J.C. & Roper, Q. (2006). Nonlinear backward stimulated Raman scattering from electron beam acoustic modes in the kinetic regime. *Phys. Plasmas* **13**, 072701.

https://doi.org/10.1017/S0263034616000495 Published online by Cambridge University Press